Acinetobacter baumannii defends against oxidative stress through a Mn^{2+}-dependent small RNA-mediated suppression of type VI secretion system

Somok Bhowmik,[1] Avik Pathak,[1] Kuldip Devnath,[1] Tarun Kumar Sharma,[3,4] Ramandeep Singh,[3] Saurabh Chugh,[3] and Ranjana Pathania[1,2,5,*]

[1]Department of Biosciences and Bioengineering, Indian Institute of Technology Roorkee, Uttarakhand-247667, India

[2]Centre of Excellence in Disaster Mitigation and Management, Indian Institute of Technology Roorkee, Uttarakhand-247667, India

[3]Translational Health Science and Technology Institute, Faridabad, Haryana-121001, India

[4]Present address: Department of Medical Biotechnology, Gujarat Biotechnology University, Gujarat-382355, India

[5]Lead Contact

*Correspondence: ranjana.pathania@bt.iitr.ac.in

Running title: A Mn^{2+}-dependent sRNA-mediated repression of T6SS

SUMMARY

Acinetobacter baumannii employs a plethora of strategies during infection to compete with other pathogens and mitigate host-mediated oxidative stress. *A. baumannii* utilizes the type VI secretion system (T6SS) to induce contact-dependent killing off the competitor microbes. However, the role of T6SS during host-induced oxidative stress is not explored in *A. baumannii*. Here, we show that *A. baumannii* T6+ cells cannot cope with phagocytic cell-mediated oxidative stress due to inadequate uptake of Mn^{2+}, which is crucial for bacterial physiology and reactive oxygen species (ROS) breakdown. Deleting the Mn^{2+}-uptake system (MntH) causes a significant increase in the T6+ population, stipulating a deleterious effect on

T6SS modulation in *A. baumannii*. Intriguingly, we identify a bonafide sRNA, AbsR28, that meditates the crosstalk between MntH and T6SS. This work elucidates a detailed mechanism of Mn^{2+}-dependent AbsR28-mediated post-transcriptional repression of T6SS, exploited by *A. baumannii* to survive in the host and establish pathogenesis.

Keywords: Mn^{2+}-uptake, MntH, manganese, sRNA, AbsR28, post-transcriptional regulation, phagocytic cell, oxidative stress, bacterial pathogenesis, pneumonia

INTRODUCTION

Acinetobacter baumannii is a Gram-negative pathogen and has gained importance due to its ability to cause wound and burn infections, sepsis, meningitis, urinary tract infection, bloodstream infection, and ventilator-associated pneumonia (Bergogne-Berezin and Towner, 1996; Dexter et al., 2015; Falagas et al., 2006; Munoz-Price et al., 2010; Peleg et al., 2008). Treating hospital-acquired *A. baumannii* infections is a major issue because most *A. baumannii* clinical strains are multidrug-resistant (MDR) (Kaye and Pogue, 2015). Due to this severe global impact on public health, it is essential to identify molecular machinery adapted by *A. baumannii* to escape from host-mediated immune responses and establish pathogenesis to design new treatment strategies.

One of the vital host-mediated immune responses pathogens come across is the neutrophil-mediated free metal ions limitation and generation of ROS at the site of infection termed “host-mediated nutritional immunity” (Hood and Skaar, 2012; Porcheron et al., 2013). Mn^{2+} sequestration by neutrophils at the site of infection reduces bacterial superoxide dismutase (SOD) and catalase activity which bacteria utilize to break down ROS (Hood and Skaar, 2012; Kehl-Fie et al., 2011). To acquire Mn^{2+} required for survival under oxidative stress and metabolism and regulation of various virulence factors, *A. baumannii* utilizes a high-affinity Mn^{2+} acquisition system *mumT* (mentioned as *mntH* in the current study as per other literature; manganese transporter H^{+}-dependent) against neutrophil-mediated metal sequestration (Juttukonda et al., 2016).

Recently, a synergism between Mn^{2+}-transporter and type VI secretion system (T6SS) has been observed in *Burkholderia thailandensis,* which helps to counter oxidative stress (Si et al., 2017b). T6SS is one of the robust secretion systems utilized by pathogens to deliver toxins into competitors or promote contact-dependent killing (Cao et al., 2016; García-Bayona et al., 2017; Souza et al., 2015; Vassallo et al., 2017). Although Mn^{2+}-uptake systems have been reported as one of the major virulence factors in Gram-negative and Gram-positive pathogens (Juttukonda and Skaar, 2015; Kehres and Maguire, 2003), crosstalk of Mn^{2+}-transporter (*mntH*) and T6SS remains unknown in *A. baumannii*.

The dynamics of T6SS assembly is an enormous and energetically expensive process for bacteria (Basler, 2015). As a contact-dependent system with specific cellular targets (Silverman et al., 2012), its expression must be precisely regulated transcriptionally and post-transcriptionally (Bernard et al., 2010; Silverman et al., 2012). Negative transcriptional regulation of T6SS by *tetR*-like regulators is observed in *A. baumannii* (Weber et al., 2015), but the mechanistic details are unknown. The major players in post-transcriptional regulation in bacteria are small regulatory RNAs (sRNAs). The sRNAs are mostly 50-500 nucleotides long, function as global regulators of numerous bacterial physiological processes, and play a crucial role in regulating several virulence factors (Gripenland et al., 2010; Romby et al., 2006). The sRNAs bind to their cognate mRNA and modulate the translational activity and/or the stability of that particular mRNA with the assistance of RNA chaperone Hfq (Franze de Fernandez et al., 1968; Schuppli et al., 2000). Recent studies demonstrated the sRNA-mediated post-transcriptional regulation of T6SS in bacteria. However, sRNA-mediated regulation of T6SS modulation in *A. baumannii* is not explored yet.

In this work, we set out to investigate the effect of T6SS expression in *A. baumannii*'s survival under oxidative stress, to check the crosstalk between Mn^{2+}-transporter and T6SS, to understand the detailed molecular mechanism of the crosstalk and its relevance in pathogenesis in the host. Herein, we show that *A. baumannii* T6+ cells grow poorly under oxidative stress owing to insufficient intracellular Mn^{2+}. We observed that deletion of MntH increases the proportion of T6+ cells in a population, showing a detrimental influence on T6SS

regulation in *A. baumannii*. We elucidate that the uptake of Mn^{2+} by MntH is necessary for AbsR28-mediated post-transcriptional suppression of T6SS to counter phagocytic cell-mediated oxidative stress and establish pathogenesis in a mouse pneumonia model.

RESULTS

A. baumannii T6+ cells are susceptible to oxidative stress due to inadequate intracellular Mn^{2+}.

Over the past few years, several studies have demonstrated the role of T6SS in bacteria in the acquisition of metal ions which helps the bacteria to survive within-host niches in metal-limited conditions (Lin et al., 2017; Si et al., 2017a; 2017b). To assess the role of T6SS in *A. baumannii*'s survival under phagocytic cell-mediated oxidative stress, we infected the phagocytic cell (human blood-derived neutrophil and macrophage RAW 264.7 cell line) with isolated wild-type (WT) T6- and T6+ cells separately. WT T6- and WT T6+ cells were isolated from the *A. baumannii* population based on Hcp (hemolysin-coregulated protein) secretion by Hcp-ELISA followed by Hcp-Western blot where cells that expressed Hcp were considered as T6SS+ (WT T6+) and the cells that showed no detectable Hcp were considered as T6SS- (WT T6-) (Figure S1A). To our surprise, WT T6- cells exhibited ~60-70% survival, whereas WT T6+ cells exhibited only ~20-30% survival against phagocytic cell-mediated killing compared to their respective untreated controls (Figure 1A and S1B). This suggests that WT T6+ cells cannot withstand phagocytic cell-mediated oxidative stress. To investigate the role of T6SS in *A. baumannii* during oxidative stress, we performed a growth assay of WT T6- and WT T6+ cells in nutrient-rich media (LB broth) supplemented with 250 µM methyl viologen (MV) to induce oxidative stress (Ahn et al., 2016; Coady et al., 2015; Hassan and Fridovich, 1977) and measured the OD_{600} at the indicated time points. The deletion mutant of TssM (a structural component of T6SS) does not express T6SS in *A. baumannii* (Repizo et al., 2015; Weber et al., 2013). So a deletion mutant of *tssM* in *A. baumannii* (Δ*tssM*) was used as a T6- control in this growth assay. All the three strains displayed equal growth in only LB, but when MV was added, WT T6+ cells exhibited a significant growth defect (Figure 1B). This strengthens our

previous observation that WT T6+ cells display enhanced sensitivity to oxidative stress compared with WT T6- cells. Intracellular ROS generation is a hallmark of an oxidative stress response (Hong et al., 2019; Schieber and Chandel, 2014). Next, we measured intracellular ROS generation in both the WT T6- and WT T6+ cells in either LB broth or LB broth supplemented with MV (250 µM). A significant increase in ROS generation was observed in WT T6+ cells compared to WT T6- cells treated with MV (Figure 1C), suggesting that WT T6+ cells are more sensitive to oxidative stress due to higher intracellular ROS accumulation. To survive against oxidative stress and host-mediated metal limitation, *A. baumannii* employs specialized metal uptake systems such as TonB-transporter, ZnuABC transporter, and MntH-transporter for the acquisition of $Fe^{2+/3+}$, Zn^{2+} and Mn^{2+}, respectively (Hood et al., 2012; Juttukonda et al., 2016; Mortensen and Skaar, 2013; Zimbler et al., 2013). Due to the compromised survival of WT T6+ cells in phagocytic cell-mediated killing, we hypothesized that WT T6+ cells are defective in uptaking of free metal ions and cannot utilize them to break down the ROS. To test this hypothesis, we infected neutrophils with WT T6- and WT T6+ cells separately and checked the expression of *mntH*, *znuB*, and *tonB* transcripts involved in Mn^{2+}-uptake, Zn^{2+}-uptake, and $Fe^{2+/3+}$-uptake, respectively, by quantitative reverse transcription PCR (qRT-PCR). There was no significant difference in the transcription of *znuB* and *tonB* genes, but in the case of *mntH* transcript, ~3.5-log2 fold reduction was observed in WT T6+ cells with respect to WT T6-cells (Figure 1D). Due to the fold reduction of *mntH* transcript in WT T6+ cells, we assumed there would be intracellular Mn^{2+} deficiency in WT T6+ cells under oxidative stress. To examine this, we grew both the WT T6- and WT T6+ cells in minimal media (M9-media) containing Casamino acid as a nutrient source (carbon) supplemented with either MV or $MnCl_2$ or both (100 µM) and measured intracellular Mn^{2+} concentration by inductively coupled plasma mass spectrometry (ICP-MS). The WT T6+ cells had ~3-fold lower Mn^{2+} levels in cell pellets than WT T6- cells (Figure 1E). In contrast, there were no significant differences in Zn^{2+} and $Fe^{2+/3+}$ levels in cell pellets of WT T6+ cells compared to the WT T6- cells (Figure S1C) when grown in M9-media containing Casamino acid supplemented with MV+$ZnSO_4$ and MV+$FeCl_3$ (100 µM), respectively. Next, we wanted to check if the

supplementation of metal ions (i.e., Mn^{2+}, Zn^{2+}, and $Fe^{2+/3+}$) could revert the growth of WT T6- and WT T6+ cells under oxidative stress. To assess this, WT T6- and WT T6+ strains were grown in nutrient-rich media (LB broth) in the presence of MV (150 µM) and supplemented with either $MnCl_2$, $ZnSO_4$, or $FeCl_3$. The WT T6- strain grew almost equally in all conditions, whereas supplementation of $ZnSO_4$ and $FeCl_3$ reverted the growth of WT T6+ cells to some extent, but supplementation of $MnCl_2$ did not revert the growth (Figure 1F, Figure S1D, and S1E). Taken together, these data suggest that WT T6+ cells display impaired growth under oxidative stress due to defects in Mn^{2+}-uptake, which is required as a cofactor for SOD and catalase to break down intracellular ROS.

A. baumannii ATCC 17978 strain contains pAB3 plasmid, which represses the T6SS through *tetR*-like regulators present in that plasmid and upon losing the plasmid, *A. baumannii* T6- cells switch to T6+ cells (Weber et al., 2015). First, we checked the presence of pAB3 plasmid and *hcp* in both the isolated WT T6- and WT T6+ cells by PCR, and no band for both the *tetR1* and *tetR2* in WT T6+ cells confirmed the loss of pAB3 which was consistent with the previous observation (Figure S2A). Next, we wanted to test whether the presence of pAB3 affects sensitivity to oxidative stress. To check this, we transformed pAB3 into the WT T6+ competent cells, confirmed the transformants (Figure S2B), and assessed the growth of WT T6-, WT T6+, and WT T6+-pAB3 in LB supplemented with MV (250 µM). Interestingly, all the three strains displayed equal growth in only LB, but when MV was added, both the WT T6+ and WT T6+-pAB3 cells exhibited a significant growth defect compared with WT T6- cells (Figure S2C). This confirms that pAB3 has no role in mediating sensitivity to oxidative stress.

Deletion of *mntH* in *A. baumannii* results in more T6+ cells in the population under oxidative stress.

Mn^{2+} is an essential micronutrient for bacterial physiology, virulence, and survival against oxidative stress (Juttukonda and Skaar, 2015). Recently, it has been observed in *B. thailandensis* that T6SS secretes an effector protein TseM that scavenges extracellular Mn^{2+} and thus helps Mn^{2+}-transporter to take up extracellular Mn^{2+} under oxidative stress (Si et al.,

2017b). However, any crosstalk of Mn^{2+}-transporter and T6SS in *A. baumannii* is not yet established, and we observed that WT T6+ cells cannot uptake extracellular Mn^{2+}. So we were curious to know the effect of Mn^{2+}-transporter (*mntH*) on T6SS under oxidative stress. To evaluate this, we created a deletion mutant of *mntH* in *A. baumannii* ATCC 17978 (Δ*mntH*), grew both the WT T6- and Δ*mntH* cells in LB supplemented with $MnCl_2$ (250 µM) to an OD_{600} of 0.6 (mid-log phase), incubated with MV (250 µM) and checked the expression of *hcp* transcript by qRT-PCR. Hcp is a structural component of T6SS and a hallmark for the expression of T6SS (Figure 2A). Interestingly, we observed ~6-log2 fold upregulation of *hcp* transcript in Δ*mntH* cells with respect to WT T6-cells (Figure 2B). The data was further validated by Hcp-Western Blot, where Hcp expression was highly induced in Δ*mntH* cells with compare to WT T6- cells in both cell lysate (CL) and culture supernatant (S) (Figure 2C). To determine the T6SS-mediated killing of prey cells by WT T6- and Δ*mntH* cells (predator/killer cells), we performed a prey-predator assay in three different ways (counting the CFU of survived prey cells, spot assay, and measuring the GFP of prey cells) using *E. coli* J53, *E. coli*-pNYL GFP, and *Pseudomonas aeruginosa* PAO1 as prey cells. As expected, Δ*mntH* cells exhibited an efficient increase in the killing of prey cells in all three assays compared to WT T6- cells (Figure 2D-F). Next, we wanted to quantify the percentage of bacteria that switch from T6- cells to T6+ cells under oxidative stress. To determine this, we grew the WT T6- and Δ*mntH* cells in LB supplemented with $MnCl_2$ (250 µM) to an OD_{600} of 0.6 (mid-log phase), incubated with MV (250 µM) for 2 h, and performed Hcp-ELISA. The percentage of switching to T6+ in Δ*mntH* cells was ~50% of the total population, whereas only ~5% of the total population was T6+ in WT T6- cells (Figure 2G and S3B). Together these data suggest that, unlike *B. thailandensis*, there is a negative impact of MntH expression on T6SS modulation in *A. baumannii* under oxidative stress.

AbsR28 mediates the crosstalk between *mntH* and T6SS in *A. baumannii*.

In bacteria, sRNAs are the major stress response post-transcriptional regulators (Holmqvist and Wagner, 2017). As the deletion of *mntH* in *A. baumannii* displayed an upregulation of

T6SS under oxidative stress, we wondered if this might be because of some sRNA-mediated post-transcriptional regulation triggered upon deletion of *mntH*. In 2014, the presence of thirty-one putative sRNAs in *A. baumannii* was predicted using bioinformatic analysis, and out of these thirty-one, three sRNAs were validated by Northern blot and RACE mapped (Sharma et al., 2014). To test our hypothesis as well as to assess their role in T6SS regulation, if any, we checked the expression of five sRNAs (out of these thirty-one) and *hfq* at the transcription level in WT T6-, WT T6+, and Δ*mntH* cells grown in LB broth supplemented with $MnCl_2$ (250 µM) followed by incubation with MV (250 µM) using qRT-PCR. Intriguingly, the expression of only one sRNA, AbsR28, showed a significant fold reduction in both the WT T6+ and Δ*mntH* cells (~3 and ~4 log2 fold reduction in WT T6+ and Δ*mntH* cells, respectively) compared with WT T6- cells (Figure 3A). Due to the fold reduction of AbsR28 transcript in WT T6+ cells and sequence conservation amongst *Acinetobacter* sp. (Figure S4A), we focused our study on evaluating the role of AbsR28 in *A. baumannii* T6SS regulation under oxidative stress. To identify genes regulated by AbsR28, we created a deletion mutant of AbsR28 in *A. baumannii* ATCC 17978 (ΔAbsR28), confirmed no polar effect (Figure S4B and S4C), and performed RNA-seq analysis comparing the relative abundance of total mRNA transcripts of WT T6- and ΔAbsR28 cells grown in LB supplemented with $MnCl_2$ (250 µM) to an OD_{600} of 0.6 (mid-log phase) and treated with MV (250 µM) for 2 h. In comparison between WT T6- and ΔAbsR28 strain, the expression of five structural genes of T6SS (A1S_1296, A1S_1298, A1S_1299, A1S_1300, and A1S_1304) and six genes encoding VgrGs/T6SS effectors molecules (A1S_0086, A1S_0550, A1S_0551, A1S_1290, and A1S_3363) displayed a significant fold-induction in ΔAbsR28 strain (Figure 3B). Further, we checked the expression of all the structural genes of T6SS in WT T6- and ΔAbsR28 strain grown in LB supplemented with $MnCl_2$ (250 µM) to an OD_{600} of 0.6 (mid-log phase) and treated with MV (250 µM) for 2 h by qRT-PCR. All the transcripts encoding for T6SS displayed a significant fold-increase in ΔAbsR28 cells compared to WT T6- cells indicating that AbsR28 negatively regulates T6SS in *A. baumannii* under oxidative stress (Figure 3C). Next, we wanted to determine whether AbsR28 directly regulates T6SS in *A. baumannii* and the importance of Mn^{2+} in this regulation. To

evaluate this, we cloned AbsR28 under an arabinose inducible promoter in pWBAD30 vector and complemented the ΔAbsR28 strain to check the expression of Hcp under oxidative stress with or without the presence of Mn^{2+}. We observed that the elevated level of AbsR28 due to arabinose pulse, decreased the expression of Hcp, and the expression of Hcp was significantly reduced when grown in the presence of Mn^{2+} in ΔAbsR28-pWBAD30AbsR28 strain (Figure 3D-F). This indicates that AbsR28 represses T6SS in *A. baumannii* under oxidative stress supplemented with $MnCl_2$. Next, we hypothesized that Mn^{2+} might bind to AbsR28 and alters its native structure which might be required for its function. Isothermal titration calorimetry (ITC) assay exhibited sequential binding affinities (*K*) of $K_1 = 1.28\times10^5 \pm 1.1\times10^4$ M^{-1}, $K_2 = 3.08\times10^4 \pm 3.5\times10^3$ M^{-1}, and $K_3 = 7.36\times10^3 \pm 4.1\times10^2$ M^{-1} indicating that Mn^{2+} binds to AbsR28 and the binding is thermodynamically favorable (Figure 3G and S5B). To determine whether the binding of Mn^{2+} affects the native structure of AbsR28, we performed in-vitro structural probing with 5'-end labeled [γ-^{32}P]ATP AbsR28 using lead acetate (PbAc), which potentially cleaves the RNA flexible regions. This structural probing was done in a modified structure buffer with an increasing concentration of $MnCl_2$. Mn^{2+}-dependent changes were observed in the gel (Figure 3H), which were not obvious in the presence of $MgCl_2$ and $ZnSO_4$ (Figure S5C). Interestingly, we observed that a region of AbsR28 (G82 to C89) has an almost similar sequence with a region of Mn^{2+}-sensing *yybP-ykoY* riboswitch (G38 to C45) (Figure 3I), which is shown to be involved in Mn^{2+}-binding (Price et al., 2015). Taken together, these data confirm that Mn^{2+} binds to AbsR28 and alters its native structure, which is needed for T6SS modulation.

Mn^{2+} is required for AbsR28 to interact with *tssM* mRNA.

sRNAs regulate the expression of target mRNA by direct complementary base-pairing with it (Balasubramanian and Vanderpool, 2013). Since T6SS in *A. baumannii* is a large gene cluster (Cianfanelli et al., 2016), we used the CopraRNA bioinformatics tool to predict the targets of AbsR28 in *A. baumannii*. CopraRNA search using whole-genome sequences of *A. baumannii* ATCC 17978 and full-length AbsR28 as inputs suggested base pairing between *tssM* and

AbsR28 with a predicted hybridization energy value of -14.10 kcal/mol (Figure 4A). To further test for direct interaction between AbsR28 and *tssM*, an in-vitro RNA-RNA interaction study was performed using a gel retardation assay. The addition of full-length AbsR28 at increasing concentrations to *tssM* resulted in retardation of *tssM* in a native gel when $MnCl_2$ was added to the structure buffer (Figure 4B). To our surprise, the retardation of *tssM* was very weak under the same condition except for the structure buffer containing $MgCl_2$ (Figure 4C and 4D). Collectively, these findings indicate that the base-pairing of AbsR28 and *tssM* is Mn^{2+}-dependent.

AbsR28 potentiates RNase E mediated degradation of *tssM* mRNA and represses T6SS.

To study the detailed molecular mechanism of AbsR28 meditated T6SS repression in *A. baumannii*, we checked the effect of AbsR28 on the stability of target RNA (i.e., *tssM*) by in-vivo pulse expression study. *A. baumannii* ΔAbsR28 strain carrying pWBAD30-AbsR28 or pWBAD30 were grown in LB supplemented with $MnCl_2$ (250 µM) to an OD_{600} of 0.6 (mid-log phase) and treated with MV (250 µM) for 2 h, cells were harvested and induced the expression of AbsR28 by adding L-arabinose (0.2% final conc. v/v). Rifampicin (400 µg/mL) was added to the samples, and then total RNA samples were collected at the indicated time points and monitored for *tssM* levels using qRT–PCR. Our data reveal that expression of AbsR28 in the presence of $MnCl_2$ significantly reduces the stability of *tssM* mRNA in vivo (Figure 4E). It has been reported that base-pairing of trans-acting sRNA with its target mRNA potentiates RNase E mediated degradation of the target mRNA in an Hfq-dependent manner and represses the translation. We hypothesized that this might also be happening in our case, where AbsR28 base-pairs with *tssM* mRNA, triggers RNase E mediated degradation of *tssM,* hence represses T6SS in *A. baumannii*. To examine this, we performed in vitro RNase E mediated degradation assay where the 5'-end of the in vitro transcribed *tssM* was labeled with [γ-^{32}P]ATP and incubated with RNase E in the presence or absence of unlabeled AbsR28 and *A. baumannii* Hfq72 or *E. coli* Hfq protein. RNase E alone cleaves *tssM*, but the cleavage is prominent in the presence of AbsR28. As expected, in the presence of AbsR28 and Hfq, the

RNase E-mediated degradation of *tssM* is more evident than alone (Figure 4F). Taken together, these data indicate that AbsR28 represses T6SS in *A. baumannii* through base-pairing with *tssM* mRNA in the presence of Mn^{2+} followed by RNase E mediated degradation of *tssM*.

Mn^{2+}-dependent AbsR28 mediated T6SS repression is required for *A. baumannii* to survive in the host and establish pathogenesis.

To understand the significance of Mn^{2+}-dependent AbsR28 mediated T6SS repression in *A. baumannii* pathogenesis, we infected the human blood-derived neutrophils with WT T6-, WT T6+, Δ*mntH*, and ΔAbsR28 cells separately and checked their survival. Consistent with our previous observation, WT T6- cells exhibited ~85% survival, whereas WT T6+ cells showed only ~40% survival against neutrophil-mediated killing compared with their respective untreated cells. In contrast, Δ*mntH* and ΔAbsR28 cells exhibited ~60% and ~40% survival, respectively (Figure 5A). This suggests that Mn^{2+}-dependent AbsR28 mediated T6SS repression in *A. baumannii* is required to withstand phagocytic cell-mediated oxidative stress. We next assessed the role of AbsR28 mediated T6SS regulation in a mouse model of *A. baumannii* pneumonia. The WT T6-, WT T6+, Δ*mntH*, and ΔAbsR28 strains were intranasally inoculated in BALB/c mice (n=8 for each group). After 36 h of post-infection, bacterial organ burden was enumerated in both lungs and liver. WT T6+, Δ*mntH*, and ΔAbsR28 strains had significantly reduced burdens in the lungs and liver (Figure 5B) compared with the WT T6- strain. Lungs isolated from the mice infected with WT T6- strain exhibited a significant tissue infiltration as indicated by necrosis and alveolar inflammation, whereas the mice lungs infected with either WT T6+, Δ*mntH*, and ΔAbsR28 strains did not show any significant damage (Figure 5C). We checked the Hcp expression in the lung homogenates isolated from the infected mice and observed high Hcp expression in WT T6+, Δ*mntH*, and ΔAbsR28 strains infected lungs, whereas WT T6- strains infected lungs showed no detectable Hcp (Figure S7A). These results demonstrate the crucial role of AbsR28 in T6SS repression to establish *A. baumannii* infection in the host.

DISCUSSION

During bacterial infection, the host recruits phagocytic cells at the site of infection, which creates oxidative stress. In addition, neutrophils sequester free metal ions at the site of infection by secreting proteins with a high affinity for metal ions (Monteith and Skaar, 2021; Murdoch and Skaar, 2022; Juttukonda et al., 2016; Weinberg, 1975). Bacteria also utilize T6SS to counter oxidative stress and host-mediated free metal restriction (Lin et al., 2017; Si et al., 2017a; 2017b). However, the role of T6SS in *A. baumannii* to survive under phagocytic cell-mediated oxidative stress is not explored yet. Our study reveals that *A. baumannii* cells which express T6SS (WT T6+), are sensitive to oxidative stress due to inadequate uptake of Mn^{2+} which is required to break down intracellular ROS generated during oxidative stress (Figure 1). This is a different observation from the recent studies, which revealed that secretion of metal scavenging effectors through T6SS helps bacteria to uptake of metal ions from the extracellular milieu and enables them to survive under oxidative stress and within-host niches in metal-limited conditions.

During oxidative stress, *B. thailandensis* secretes TseM through T6SS, which sequesters Mn^{2+} ions and helps in the uptake of Mn^{2+}, thus mediating a synergy between Mn^{2+}-uptake system and T6SS (Si et al., 2017b). But in our current study, we observed a significant fold-reduction in *mntH* expression in the WT T6+ cells, and these cells were defective in Mn^{2+}-uptake during oxidative stress (Figure 1D-F, S1D, and S1E). To check the impact of MntH on T6SS expression, we created Δ*mntH* in *A. baumannii* and observed that deletion of *mntH* promotes a significant increase in T6SS expression under oxidative stress (Figure 2), indicating a negative impact of MntH expression on T6SS modulation in *A. baumannii* under oxidative stress which is quite interesting. Next, we focused our study on determining the mechanism behind the negative regulation.

Both *tetR1* and *tetR2* (present in pAB3) are involved in T6SS repression in *A. baumannii* ATCC 17978 cells (Weber et al., 2015) but the molecular mechanism is unclear. Since the WT T6- cells switch to WT T6+ cells upon losing pAB3 and WT T6+ cells are

sensitive to oxidative stress in our current study, we speculated that the sensitivity to oxidative stress might be due to losing pAB3. We show that pAB3 has no role in conferring resistance to oxidative stress (Figure S2C), indicating the existence of an alternate Mn^{2+}-dependent T6SS regulation in *A. baumannii* under oxidative stress.

The sRNA-mediated post-transcriptional regulation of T6SS is well understood in *P. aeruginosa* (Brencic and Lory, 2009; Janssen et al., 2018; Marden et al., 2013; Romero et al., 2018). However, sRNA-mediated regulation of T6SS in *A. baumannii* is not explored yet. Since deletion of *mntH* showed a significant increase in T6SS expression in *A. baumannii* (Figure 2), we hypothesized that this might be due to some Mn^{2+}-dependent post-transcriptional repression which is effected upon the deletion of *mntH*. To examine this, we checked the expression of several sRNAs (Sharma et al., 2014) transcripts in WT T6-, WT T6+, and Δ*mntH* cells grown under oxidative stress supplemented with $MnCl_2$. We observed that the expression of one sRNA, i.e., AbsR28, was significantly reduced in both WT T6+ and Δ*mntH* cells when compared with WT T6- cells (Figure 3A). This indicates AbsR28 might mediate the crosstalk between MntH and T6SS in *A. baumannii* during oxidative stress. To strengthen our hypothesis, we observed that the elevated level of AbsR28 represses the expression of T6SS in *A. baumannii* under oxidative stress supplemented with $MnCl_2$ by pulse expression studies (Figure 3D-F). Next, we focused our study on elucidating the mechanistic details of AbsR28 mediated T6SS repression in *A. baumannii* under oxidative stress. We show that the binding of Mn^{2+} to AbsR28 alters its native structure and results in a complementary base-pairing with *tssM* transcripts (Figure 3G, 3H, and 4B). TssM is one of the vital structural components of the T6SS membrane complex and essential for T6SS assembly (Brunet et al., 2015; Felisberto-Rodrigues et al., 2011; Ma et al., 2012; Stietz et al., 2020; VanRheenen et al., 2004). Next, we wanted to assess the impact of the cognate base-pairing on *tssM* transcripts in vivo. We observed that the stability of *tssM* transcripts was significantly reduced under AbsR28 expression in the presence of Mn^{2+} (Figure 4E). In Gammaproteobacteria, RNase E is the primary catalyst of mRNA decay (Caron et al., 2010). sRNAs induce the decay of target

mRNA by RNase E-mediated mRNA degradation (Afonyushkin et al., 2005; Caron et al., 2010; Guillier and Gottesman, 2008; Morita at al., 2005; Prévost et al., 2011; Urban and Vogel, 2007; Vogel and Luisi, 2011). Since we observed AbsR28 expression-dependent decay of *tssM* transcripts in vivo, we hypothesized that AbsR28 triggers RNase E mediated processing of *tssM* transcripts. Our data demonstrate that AbsR28 potentiates RNase E-mediated degradation of *tssM* mRNA with the assistance of RNA chaperon Hfq (Figure 4F). The current study reveals how AbsR28 represses T6SS and plays a vital role in mediating the crosstalk between MntH and T6SS in *A. baumannii* under oxidative stress.

Deletion of *mntH* in *A. baumannii* strain results in impaired growth during calprotectin-mediated metal chelation and compromised survival in mice model of infection (Juttukonda et al., 2016). Based on our current observations, we speculated that this might be because of deletion of *mntH* that disrupts the uptake of Mn^{2+}, which is needed for AbR28-mediated T6SS repression during oxidative stress. To test our hypothesis, we checked the impact of Mn^{2+}-dependent AbsR28 mediated regulation of T6SS in *A. baumannii* pathogenesis. All the three stains, i.e., WT T6+, Δ*mntH*, and ΔAbsR28, were compromised in survival under neutrophil-mediated oxidative stress and less virulent in the mice suggesting that Mn^{2+}-dependent AbsR28 mediated T6SS repression helps *A. baumannii* to survive in the host (Figure 5A-C).

The T6SS is often silent in the clinical isolates of *A. baumannii* (Meumann et al., 2019; Kim et al., 2017; Traglia et al., 2018; Wright et al., 2014). The reason behind the inactive T6SS in *A. baumannii* is still questionable. The following may cause inactive T6SS in *A. baumannii* clinical isolates: (i) high energy is required for T6SS expression, so to utilize the energy for some other cellular process, T6SS is silent; (ii) T6SS components are immunogenic (Mougous et al., 2006; Zheng et al., 2010) so it might be advantageous for *A. baumannii* T6SS inactive strains to evade from the host-mediated immune response (Lopez et al., 2020); (iii*) A. baumannii* cells switch from T6- to T6+ at the cost of losing antibiotic resistance encoded by the plasmid (Weber et al., 2015) so to maintain the resistance over competing with other bacteria it might prefer to inactivate the T6SS. We also tested the presence of both AbsR28

and *hcp* in other pathogenic isolates of *A. baumannii* strains (Figure S8A) and observed that T6SS is inactive in nine strains out of eleven strains tested under oxidative stress supplemented with $MnCl_2$ (Figure S8B).

In summary, we show here the mechanistic details of AbsR28 sRNA-mediated T6SS repression in *A. baumannii* ATCC 17978 under oxidative stress (Figure 6). The sequential events of this pathway are as follows: (i) during oxidative stress, *A. baumannii* cells upregulate *mntH* to increase the uptake of Mn^{2+}; (ii) Intracellular Mn^{2+} binds to AbsR28 and alters its native structure; (iii) the altered structure of AbsR28 helps in the complementary base pairing with *tssM* mRNA transcript and triggers RNase E processing; (iv) Degradation by RNase E decreases the abundance of *tssM* transcripts and thereby represses the T6SS expression. *A. baumannii* cells that lose this controlled regulation result in T6+ cells, unable to withstand oxidative stress and are cleared by the host. The findings presented here reveal an alternate detailed molecular mechanism of sRNA-mediated T6SS regulation in *A. baumannii* ATCC 17978 apart from *tetR*-mediated regulation of T6SS (Weber et al., 2015). Our finding shows the crucial role of AbsR28 in regulating the molecular transition between T6- and T6+ phenotypes in *A. baumannii,* which is essential to survive under oxidative stress and establish pathogenesis in the host.

METHOD DETAILS

Bacterial strains and growth conditions

Bacterial strains used in this study are listed in Table 2. *A. baumannii* strains were grown at 37ºC in an incubator in LB broth or LB agar. *E. coli* J53 strains were grown in LB broth or LB agar, supplemented with 100 µg/mL sodium azide when necessary. *E. coli*-pNYL GFP strains were grown in LB broth or LB agar, supplemented with 50 µg/mL kanamycin when necessary. *P. aeruginosa* PAO1 strains were grown in LB broth or LB agar. *A. baumannii* ATCC 17978 ΔAbsR28-pWBAD30 and *A. baumannii* ATCC 17978 ΔAbsR28-pWBAD30AbsR28 strains were grown in LB broth or LB agar, supplemented with 50 µg/mL kanamycin.

Primary cell culture

All experiments using human blood-derived neutrophils under protocol BT/IHEC-612020/7865 were reviewed and approved by the Institute Human Ethics Committee (HEC) of the Indian Institute of Technology Roorkee. Blood samples were collected from healthy volunteers (Ages 28-30) in vacutainer tubes (BD Vacutainer^{R} K2E EDTA; REF367525). Neutrophils were isolated from the blood samples within 30 min of collection using Polymorphprep™ (ProteoGenix) according to the manufacturer's instructions. After isolation, the neutrophils were incubated on ice for 1 h in RPMI 1640 cell culture medium (RPMI + 10% (v/v) FBS), transferred into 12-well tissue culture plates (Thermo Fisher Scientific), and incubated in a cell culture incubator (Eppendorf) at 37ºC (5% CO_2) for 1 hour before experimentation.

Animal Models

All animal experiments under protocol BT/IAEC/2018/07 were reviewed and approved by the Institute Animal Ethics Committee of the Indian Institute of Technology Roorkee. Procedures were performed according to the institutional policies. Adult (6–8 week old) age-matched male BALB/c (procured from Indian Institute of Science Education and Research Mohali, India) mice were housed in groups of eight and maintained at IIT Roorkee Animal Facilities.

Isolation of *A. baumannii* T6- and T6+ cells

A. baumannii T6- and T6+ cells were isolated using Hcp-ELISA as described previously (Weber et al., 2013) with some modifications. Briefly, a fresh colony of wild-type *A. baumannii* ATCC 17978 streaked on LB-agar plate was used to inoculate in 5 mL LB-medium overnight (O/N) at 37ºC in shaking. 0.1% inoculum from the O/N culture was then subcultured into fresh 5 mL LB-medium and grown at 37ºC in shaking to an OD_{600} of 0.6 (mid-log phase). The culture was serially diluted in LB medium and plated on LB-agar followed by incubation at 37ºC for O/N to obtain more than 100 isolated colonies. Individual colonies were inoculated in a 96-well plate containing 200 µL of LB medium/well and incubated at 37ºC for O/N in gentle shaking. After O/N growth, the plate was centrifuged to pellet down the bacterial cells and 75 µL of the supernatant from each well was transferred to a 96-well ELISA-plate (Thermo Fisher Scientific) containing 25 µL of binding buffer (0.0258 M sodium carbonate, 0.0742 M sodium

bicarbonate, pH 9.5) in each well (for example, A1 supernatant from 96-well plate was transferred to A1 of 96-well ELISA plate). The ELISA plate was incubated at 4ºC for O/N on a gel rocker for efficient binding. The plate was then washed with 1X PBS and blocked with 200 µL of blocking solution (5% w/v skim milk in PBST; 1X PBS containing 0.1% inoculum v/v Tween-20) for 1 h at room temperature (RT). Primary anti-Hcp-antibody raised in the rabbit at a dilution of 1:10000 in blocking solution (2.5% w/v skim milk in PBST) was used at 100 µL/well to probe at 4ºC for O/N. Following three successive washes with PBST, HRP-conjugated goat anti-rabbit secondary antibody (Thermo Fisher Scientific) at a dilution of 1:20000 in a solution (1X PBS containing 0.1% inoculum v/v Tween-20) was added 100 µL/well and incubated for 1 h at RT in the dark. After three successive washes with PBST and one wash with PBS, 50 µL substrate (citrate phosphate buffer at pH 5.6 containing H_2O_2 and *o*-Phenylenediamine dihydrochloride) was added to each well and waited for 10-15 min to develop yellow color. The reaction was stopped by adding 3N HCl, which will turn yellow to orange, and measured the OD at 495 nm. Purified His_6-Hcp was used as a positive control and only LB medium as a negative control for the assay. A well that appears for the T6SS+ signal (i.e., develops orange color after ELISA) was marked and the cells from that particular well of the 96-well plate (the source of the supernatant sample) were isolated (considered at *A. baumannii* T6+ after 1st round of ELISA). Similarly, a well that appears for the T6SS- signal (i.e., does not develop any color after ELISA) was marked and the cells from that particular well of the 96-well plate (the source of the supernatant sample) were isolated (considered at *A. baumannii* T6- after 1st round of ELISA). Both the *A. baumannii* T6- and T6+ cells from 1st round ELISA were plated on LB agar and further Hcp-ELISA (2nd round) was performed using freshly isolated individual colonies to confirm the T6SS phenotype.

Further, *A. baumannii* T6+ cells were checked for Hcp secretion phenotype by Hcp-Western Blot. The *A. baumannii* T6- and T6+ cells from 2nd round ELISA were inoculated in LB medium and grew overnight (O/N) at 37ºC in shaking. 0.1% inoculum from the O/N cultures was then subcultured into fresh 5 mL LB-medium individually and grown at 37ºC in shaking to

an OD_{600} of 0.6 (mid-log phase) for both the strains. Bacterial cells were harvested from 1 mL cultures and supernatants were collected. The supernatants were filtered through a 0.22 µm syringe filter (Merk Millipore Ltd.) and concentrated using trichloroacetic acid. The pellets were dissolved in 1X SDS-gel loading dye and heated at 95ºC for 5 min. Whole-cell lysate (OD_{600} normalized volume) and supernatants were run onto 15% SDS-PAGE for separation and transferred to a PVDF membrane (Cytiva). Followed by blocking (5% w/v skim milk in PBST; 1X PBS containing 0.1% inoculum v/v Tween-20) for 1 h at RT, the membrane was probed by primary anti-Hcp-antibody raised in the rabbit at a dilution of 1:1000 in blocking solution (2.5% w/v skim milk in PBST) at 4ºC for O/N on a gel rocker. Following five successive washes with PBST, HRP-conjugated goat anti-rabbit secondary antibody (Thermo Fisher Scientific) at a dilution of 1:20000 in a solution (1X PBS containing 0.1% inoculum v/v Tween-20) was added and incubated for 1 h at RT in the dark. After five successive washes with PBST and one wash with PBS, ECL substrate (TakaRa) was added and developed onto X-ray film.

Estimation of cell survival from phagocytosis

Neutrophils were isolated from human blood as described above and diluted to obtain a final concentration of $1x10^4$ cells/well. A fresh colony of WT T6- and WT T6+ strain streaked on LB-agar plates were used to inoculate in 5 mL LB-medium for O/N at 37ºC in shaking. 0.1% inoculum from the O/N cultures were then subcultured into fresh 5 mL LB-medium and grown at 37ºC in shaking to an OD_{600} of 0.6 (mid-log phase). Bacterial cells were harvested and diluted to obtain 10^4 CFU/µL. The diluted bacterial cultures were then opsonized in fetal bovine serum (non-heat treated) for 15 minutes. Neutrophils were then co-incubated with bacterial strains at an MOI of 1:1 ratio in RPMI 1640 cell culture medium (HIMEDIA) and incubated at 37ºC in an animal tissue culture incubator (Eppendorf). The same method was performed for macrophage RAW 264.7 cell line in the DMEM medium (HIMEDIA). After 4 h of infection, the medium supernatants were serially diluted and plated onto Leeds *Acinetobacter* medium plates. After incubation at 37ºC for O/N, the bacterial colonies were enumerated and the percent growth was quantified by dividing the CFU of the particular *A. baumannii* strain-

neutrophil/macrophage RAW 264.7 cell line co-culture by that respective strain alone culture (grown in the same condition in the absence of neutrophil/macrophage RAW 264.7 cell line). Only neutrophil/ macrophage RAW 264.7 cell line were kept as a negative control for the assay.

Growth assay under oxidative stress

A fresh colony of each indicated strain streaked on LB-agar plates was used to inoculate in 5 mL LB-medium for O/N at 37ºC in shaking. 0.1% inoculum from the O/N cultures were then subcultured into fresh 5 mL LB-medium and grown at 37ºC in shaking to an OD_{600} of 0.6 (mid-log phase) for each strain. From the mid-log phase cultures, 0.1% inoculum was inoculated in a 200 µL fresh LB medium containing methyl viologen (MV) at 250 µM (final conc.). All the growth assays were performed in a sterile 96-well plate (Genaxy) at 37ºC with shaking linearly at 180 CPM (6 mm) and the OD_{600} as a measurement of growth was measured at every 30 min interval for the indicated total time in the Synergy microplate reader (BioTek). Only media without any culture served as a negative control for this assay. The represented data are after background correction.

ROS quantification

A fresh colony of WT T6- and WT T6+ strain streaked on LB-agar plates were used to inoculate in 5 mL LB-medium for O/N at 37ºC in shaking. 0.1% inoculum from the O/N cultures were then subcultured into fresh 5 mL LB-medium and grown at 37ºC in shaking to an OD_{600} of 0.6 (mid-log phase) for each strain. Bacterial cells were harvested by centrifugation and washed in sterile 1X PBS. The bacterial cell pellets were resuspended in 1X PBS and 2',7'-dichlorofluorescein diacetate (Thermo Fisher Scientific) was added at a final concentration of 100 µM. After incubation for 30 min at 37ºC, the cells were washed with 1X PBS to remove excess dye and transferred to 100 µL/well of a 96-well transparent bottom black well plate (BRAND). MV (250 µM final conc.) was added to the wells containing bacterial cells and incubated at 37ºC with shaking linearly at 180 CPM (6 mm). OD_{600} and fluorescence (excitation/emission at 485/535 nm) were measured at every 10 min interval for the indicated

total time in the Synergy microplate reader (BioTek). The represented data are after background correction and OD_{600} normalization.

Quantitative RT-PCR analysis

Human blood-derived neutrophils were co-incubated with the bacterial strains as described in the above section. After 4 h incubation, the tissue culture plate was centrifuged at 400g for 5 min to settle down the neutrophils. Sample supernatants containing the bacterial cells were collected and harvested the bacterial by centrifugation at maximum speed. After washing the cell pellet with 1X PBS, RNA was extracted from the bacterial cells by the classic phenol-chloroform method. Briefly, 1 mL RNAiso Plus reagent (TakaRa) was added to each bacterial cell pellet and mixed vigorously by pipetting. After incubation for 5 min at RT, 200 µL of chloroform was added to each sample, mixed using a vortex, and allowed to stand at RT for 15 min for phase separation. The samples were then centrifuged at 12000g for 15 min at 4ºC. After centrifugation, the upper aqueous layer of each sample was transferred to a fresh tube. RNA was precipitated by the addition of isopropyl alcohol at a 1:1 ratio, followed by incubation at RT for 10 min and centrifugation at 12000g for 10 min at 4ºC. The supernatants were removed carefully and washed the pellet by adding 1 mL of ice-chilled 70% ethanol followed by centrifugation at 12000g for 5 min at 4ºC. The supernatants were decanted carefully and air-dried the pellet. The extracted RNA was resuspended in 50 µL of pre-warmed RNase-free water. The DNA contaminations were removed by incubating the extracted RNA with DNase I (Thermo Scientific) according to the manufacturer's instructions, followed by heat inactivation. The efficiency of the DNase I treatment was confirmed by PCR using DNase I treated RNAs as a template. RNA concentrations were determined by Nanodrop (Eppendorf) and 2 µg of the total RNA for each sample was used for cDNA synthesis using PrimeScript 1st strand cDNA Synthesis Kit (TakaRa) according to the manufacturer's instructions. The synthesized cDNA was diluted to 200 µL with RNase-free water and stored at -80ºC till further use. The qRT-PCR was performed using 2X SYBR Green master mix (Thermo Fisher Scientific), primer pairs in Table 1, and cDNA as template, and after mixing well, the reactions

were transferred to a 96-well RT-PCR plate (BRAND). Amplifications were achieved using a 3-step program on a QuantStudio 5 system (Thermo Fisher Scientific). Transcript abundance was calculated using the $\Delta\Delta C_T$ method (Livak and Schmittgen, 2001) and normalized by the 16s gene.

Quantification of intracellular metal content

The concentration of metal content in bacterial cells was determined as described previously (Juttukonda et al., 2016) with some modifications. Briefly, a fresh colony of WT T6- and WT T6+ strain streaked on LB-agar plates were used to inoculate in 5 mL minimal medium (M9-medium) supplemented with 1% Casamino acids as a nutrient source for O/N at 37ºC in shaking. 0.1% inoculum from the O/N cultures were then subcultured into fresh 100 mL M9-medium (supplemented with 1% Casamino acids) supplemented with or without $MnCl_2$, $ZnSO_4$, or $FeCl_3$ at a final concentration of 100 µM and grown at 37ºC in shaking to an OD_{600} of 0.6 (mid-log phase) for each strain. Then MV was added at a final concentration of 100 µM to the culture to induce oxidative stress and grown further at 37ºC in shaking for 4 h. The bacterial cultures were then transferred to pre-weighed metal-free 50 mL centrifuge tubes and centrifuged to harvest by the cell pellet, washed thrice with Milli-Q deionized water, and dried thoroughly. The pellet weight was measured using an analytical balance (G&G). Pellets were digested with 1 mL 70% HNO_3 by using Milli-Q deionized water as a diluent for O/N at 90°C and diluted with 9 mL of 3.5% HNO_3 by using Milli-Q deionized water as diluent. The samples were then subjected to inductively coupled plasma-mass-spectrometry (8900 ICP-MS Triple Quad, Agilent) at Institute Instrumentation Centre (IIC) in IIT Roorkee. The concentrations were determined by utilizing a standard curve for each metal. Only M9-medium supplemented with 1% Casamino acids was used as a control.

Bacterial survival assay upon uptake of metal ions under oxidative stress

A fresh colony of WT T6- and WT T6+ strain streaked on LB-agar plates were used to inoculate in 5 mL minimal medium (M9-medium) supplemented with 1% Casamino acids as a sole nutrient source for O/N at 37ºC in shaking. 0.1% inoculum from the O/N cultures were then

subcultured into fresh 5 mL M9-medium (supplemented with 1% Casamino acids) supplemented with or without $MnCl_2$, $ZnSO_4$, $FeCl_3$ or all together at a final concentration of 250 µM and grown at 37ºC in shaking to an OD_{600} of 0.6 (mid-log phase) for each strain. Then MV was added at a final concentration of 250 µM to the culture to induce oxidative stress and grown further at 37ºC in shaking for 2 h. Cells were harvested from a 1 mL culture, washed with 1X PBS, and dissolved into 50 µL of 1X PBS. For spot assay, after a serial dilution in 1X PBS, 5 µL from each dilution was spotted onto LB agar containing MV at a final concentration of 100 µM alone or with $MnCl_2$, $ZnSO_4$, and $FeCl_3$ (250 µM each), incubated at 37ºC for O/N, and images were taken by gel documentation system (Biorad). A similar assay was performed with H_2O_2; in that case, the final concentration of H_2O_2 was 500 µM. For growth assay, 0.1% inoculum from the O/N cultures were then subcultured into fresh 5 mL M9-medium (supplemented with 1% Casamino acids) and grown at 37ºC in shaking to an OD_{600} of 0.6 (mid-log phase) for each strain. From the mid-log phase cultures, 0.1% inoculum was inoculated in 200 µL fresh LB medium containing methyl viologen (final concentration of 150 µM) supplemented with or without $MnCl_2$, $ZnSO_4$, or $FeCl_3$ at a final concentration of 250 µM. All the growth assays were performed in a sterile 96-well plate (Genaxy) at 37ºC with shaking linearly at 180 CPM (6 mm) and the OD_{600} as a measurement of growth was measured at every 30 min interval for the indicated total time in the Synergy microplate reader (BioTek). Only media without any culture served as a negative control for this assay. The represented data are after background correction.

Generation of knock-out strains

The deletion mutants were created using a homologous-recombination method described previously (Tucker et al., 2014) with some modifications. Briefly, a construct carrying apramycin cassette (amplified from pMDIAI and having FRT sites on both sides) flanking between 500 bp upstream and 500 bp downstream of the gene of interest was cloned into a pUC18 vector (used as a cloning vector). A PCR product was amplified from the construct using 125 bp upstream forward primer and 125 bp downstream reverse primer of the gene of

interest listed in Table 1. Around 5 µg of the concentrated PCR gel-purified product was transformed into *A. baumannii* electrocompetent cells harboring pAT02 (contains Rec_{Ab} system) under IPTG induction (2 mM) and plated on LB-agar containing apramycin (15 µg/mL). The transformants were further passaged on LB-agar containing an increasing concentration of apramycin (15-30 µg/mL). The recombinants were further confirmed by PCR using primers located outside the regions of homology (i.e., 500 bp upstream forward primer and 500 bp downstream reverse primer of the gene of interest) listed in Table 1. Following PCR confirmation and curing of pAT02, clean knockout (K/O) was created by transforming pAT03 (contains FLP recombinase system) under IPTG induction (2 mM). A loss of apramycin resistance confirmed the clean K/O and the losing apramycin-FRT was further confirmed by PCR using apramycin forward and reverse primers listed in Table 1. After curing pAT03, the clean K/O strains were maintained in glycerol (15%) at -80ºC for further use.

Bacterial killing assay

Bacterial killing assays were performed as described previously (Weber et al., 2015) with some modifications. Briefly, *A. baumannii* T6SS- and Δ*mntH* strains were used as killer/predator and *E. coli* J53 (selection marker sodium azide; 100 µg/mL) or *E. coli*-pNYL GFP (selection marker kanamycin; 50 µg/mL) or *P. aeruginosa* (selectively grow on *P. aeruginosa* agar medium) were used as prey for this assay. Fresh colonies of both *A. baumannii* T6SS- and Δ*mntH* strains streaked on LB-agar plates were used to inoculate in 5 mL LB-medium for O/N at 37ºC in shaking. 0.1% inoculum from the O/N cultures was then subcultured into fresh 5 mL LB-medium containing 100 µM MV and $MnCl_2$ and grown at 37ºC in shaking to an OD_{600} of 0.6 (mid-log phase). Cells were harvested from a 2 mL culture, washed with 1X PBS, and dissolved into 50 µL of 1X PBS. Simultaneously, the prey cells were grown in LB medium containing respective selection markers to an OD_{600} of 0.6 (mid-log phase), harvested the cells from 2 mL culture, washed with 1X PBS, and dissolved into 50 µL of 1X PBS. The predator and prey cells were mixed at a ratio of 1:1 and spotted 100 µL mixture on sterile 0.22 µm syringe filters placed on dry LB agar plates. After being air-dried inside the hood, the plates were kept at 37ºC for 4 h. The mixed cultures were scraped out and

resuspended in 1X PBS. For spot assay, after a serial dilution in 1X PBS, 5 µL from each dilution was spotted onto LB agar containing sodium azide (100 µg/mL) when *E. coli* J53 was used as prey or LB agar containing kanamycin (50 µg/mL) when *E. coli*-pNYL GFP was used as prey. The plates were incubated at 37ºC for O/N and images were taken using a camera. For CFU count, after a serial dilution in 1X PBS, 100 µL from each dilution was spread onto LB agar containing sodium azide (100 µg/mL) when *E. coli* J53 was used as prey or LB agar containing kanamycin (50 µg/mL) when *E. coli*-pNYL GFP was used as prey or *P. aeruginosa* agar medium when *P. aeruginosa* was used as prey. The plates were incubated at 37ºC for O/N and counted the number of colonies. The survival percentage of the prey cells was calculated considering the CFU of alone prey cells as 100%. To measure the prey cells' GFP fluorescence, both the predator and prey cells were mixed at a 1:1 ratio in LB-medium in a 96-well transparent bottom black well plate (BRAND). GFP fluorescence was recorded at 485/525 nm to measure prey cells' growth at 37ºC every 3 h.

Western Blot analysis for Hcp

A fresh colony of each indicated strain streaked on LB-agar plates was used to inoculate in 5 mL LB-medium for O/N at 37ºC in shaking. 0.1% inoculum from the O/N cultures were then subcultured into fresh 5 mL LB-medium containing $MnCl_2$ at a final concentration of 250 µM and grown at 37ºC in shaking to an OD_{600} of 0.6 (mid-log phase) for each strain. MV was added to the culture at a final concentration of 250 µM and incubated for another 2 h. Hcp secretion phenotype of the strains was performed by Hcp-Western Blot as described above. Primary anti-Hfq-antibody raised in rabbit at a dilution of 1:1000 was used as a control for cell lysate (CL).

ELISA assay for HCP

A fresh colony of each indicated strain streaked on LB-agar plates was used to inoculate in 5 mL LB-medium for O/N at 37ºC in shaking. 0.1% inoculum from the O/N cultures were then subcultured into fresh 5 mL LB-medium containing $MnCl_2$ at a final concentration of 250 µM and grown at 37ºC in shaking to an OD_{600} of 0.6 (mid-log phase) for each strain. MV was

649 added to the culture at a final concentration of 250 µM and incubated for another 2 h. The rest
650 of procure for Hcp-ELISA was performed as mentioned above.

651 **RNA-sequencing data analysis**

652 RNA was isolated from WT T6- and ΔAbsR28 cells grown in LB supplemented with $MnCl_2$
653 (250 µM) to an OD_{600} of 0.6 (mid-log phase), treated with MV (250 µM) for 2 h, and purified as
654 described above. RNA sequencing was performed by Biokart India Pvt. Ltd. (India) using the
655 Illumina HiSeq 4000 platform (Illumina). RNA integrity was determined using RNA
656 ScreenTape System (Agilent) and 4150 TapeStation System (Agilent). The RNA
657 concentration was determined on Qubit 3.0 Fluorometer (ThermoFisher Scientific) using the
658 Qubit RNA Assay Kit (ThermoFisher Scientific). rRNA was depleted using the QIAseq
659 FastSelect−5S/16S/23S Kit (Qiagen) and cDNA libraries were prepared with KAPA RNA
660 Hyaperprep kit KR1350 – v2.17 (Roche). Data quality was checked by Fastqc v0.11.8. Data
661 trimming and adapter removal were performed by Trim Galore v 0.6.7. Analysis was performed
662 by Rockhopper v 2.0.3. Comparative and statistical analyses were performed using iGeak
663 v1.0a using the reference *A. baumannii* ATCC 17978 genome (NCBI: CP000521.1).

664 **Pulse expression studies**

665 An arabinose inducible vector pWBAD30 was modified from the pBAD30 backbone for this
666 study. Briefly, the kanamycin cassette from the pKD4 plasmid was cloned into the PvuI site
667 on the AmpR gene in pBAD30. The forward primer of the kanamycin cassette contained the
668 XhoI site for cloning of *A. baumannii* compatible ori (named pW) into vector. After completion
669 of two cloning, the sRNA was cloned at the EcoRI and HindIII sites present at the MCS of the
670 plasmid, tightly controlled by arabinose inducible promoter. The pWBAD30-AbsR28 plasmid
671 was transformed into ΔAbsR28 electrocompetent cells and the transformants were selected
672 on LB-agar plates containing kanamycin (50 µg/mL). ΔAbsR28 transformed with pWBAD30
673 served as a vector control. For survival assay, fresh colonies of the indicated strains streaked
674 on LB-agar plates containing kanamycin (50 µg/mL) were used to inoculate in 5 mL LB-
675 medium containing kanamycin (50 µg/mL) or O/N at 37ºC in shaking. 0.1% inoculum from the

O/N cultures was then subcultured into fresh 5 mL LB-medium with kanamycin (50 µg/mL) containing $MnCl_2$ at a final concentration of 250 µM and grown at 37ºC in shaking to an OD_{600} of 0.6 (mid-log phase). MV (250 µM final conc.) was added to the culture and grown for another 2 h. Cells were harvested from a 2 mL culture, washed with 1X PBS, and dissolved into 50 µL of 1X PBS. Simultaneously, *E. coli* J53 as prey cells were grown in LB medium containing sodium azide (100 µg/mL) to an OD_{600} of 0.6 (mid-log phase), harvested the cells from 2 mL culture, washed with 1X PBS, and dissolved into 50 µL of 1X PBS. The predator and prey cells were mixed at a ratio of 1:1, arabinose (0.2% v/v final concentration) was added for AbsR28 expression, and spotted the 100 µL mixture on sterile 0.22 µm syringe filters, placed on dry LB agar plates. After being air-dried inside the hood, the plates were kept at 37ºC for 4 h. The mixed cultures were scraped out and resuspended in 1X PBS. After a serial dilution in 1X PBS, 100 µL from each dilution was spread onto LB agar containing sodium azide (100 µg/mL). The plates were incubated at 37ºC for O/N and counted the number of colonies. The survival percentage of the prey cells was calculated considering the CFU of alone prey cells as 100%. To check gene expression by qRT-PCR, the cells were grown in LB containing $MnCl_2$ at a final concentration of 250 µM and grown at 37ºC in shaking to an OD_{600} of 0.6 (mid-log phase). MV (250 µM final conc.) and arabinose (0.2% v/v final concentration) were added to the media and incubated for a further 4 h. RNA were extracted and qRT-PCR was performed as described above. For Hcp-Western Blot, the cells were grown in LB containing $MnCl_2$ at a final concentration of 250 µM and grown at 37ºC in shaking to an OD_{600} of 0.6 (mid-log phase). MV (250 µM final conc.) and arabinose (0.2% v/v final concentration) were added to the media and incubated for a further 4 h. Cell lysate (CL) and cell-free supernatant (S) were run in SDS-PAGE and performed Western Blot as mentioned above.

Isothermal calorimetry

All ITC titrations were performed using ITC-200 (GE Healthcare). After degassing, 600 µM $MnCl_2$ was placed into the syringe and 30 µM in vitro transcribed AbsR28 was placed in the reaction cell. ITC was performed over 20 injections, each 1.8 µl of $MnCl_2$ with an interval of

120 s allowed for equilibration of the mixture between injections at a constant stirring of 500 rpm. All reactions were performed in buffer containing 10 mM Tris, 100 mM KCl, pH 8.0 at 25ºC. Using the Origin version 7.0 software thermogram provided with the system, data were fitted as a sequential binding model with binding constant (*K*) after subtracting the control data.

In vitro RNA transcription and 5'-end labeling

In vitro transcription (IVT) was performed as described earlier (Desnoyers and Massé, 2012). Template DNA for IVT was obtained by using *A. baumannii* ATCC 17978 genomic DNA as a PCR template and forward primers containing the T7 promoter listed in Table 1. T7 transcription was performed using the T7 RNA polymerase (Thermo Scientific) according to the manufacturer's instructions. DNA contaminations were removed by incubating the transcript RNA with DNase I (Thermo Scientific) according to the manufacturer's instructions, followed by heat inactivation. Complete transcripts were obtained by phenol-chloroform extraction, running long Urea-PAGE followed by gel purification and concentrated by sodium acetate precipitation. To perform 5'-end labeling, transcripts were dephosphorylated with FastAP (Thermo Scientific) and 5'-labeled with [^{32}P]-γ-ATP using T4 polynucleotide kinase (Thermo Scientific) with forward reaction buffer according to the manufacturer's protocol. Radiolabeled transcripts were purified by running long Urea-PAGE followed by gel purification and concentrated by sodium acetate precipitation.

In vitro structural probing

In vitro structural probing was performed as described earlier (Dambach et al., 2015) with some modifications. Briefly, in vitro transcribed 5'-labeled AbsR28 (2.5 pmol) were denatured for 2 min at 65ºC, incubated on ice for 5 min, and RT for 5 min. AbsR28 was then incubated in a modified 2X in-line buffer (100 mM Tris-HCl pH 8.3, 200 mM KCl) at a range of $MnCl_2$ concentration containing yeast tRNA (1 µg/reaction) for 40 h at room temperature. Afterward, 2 µL from 25 mM lead(II) acetate stock was added to each of the 10 µL reactions and incubated for an exact 2 min at 37ºC. RNaseT1 ladder was generated by incubating 5'-labeled AbsR28 with RNaseT1 (0.1 U/µL and 1.0 U/µL) in 1X sequencing buffer (Ambion) for 3 min at

55ºC. Alkaline RNA ladders were generated by incubating 5'-labeled AbsR28 in 1X alkaline buffer (Ambion) for 5 min at 90ºC. All reactions were stopped immediately by adding a stop buffer (Ambion). After phenol:chloroform:isoamyl alcohol purification, RNA pellets were dissolved in loading buffer II (Ambion). All samples were denatured for 3 min at 95ºC and loaded on 10% PAGE/7 M urea sequencing gels at a constant 15 Watt. After gel drying for 2 h at 80ºC, bands were visualized using a phosphoimager (Typhoon FLA 7000, GE Healthcare) and ImageQuant software.

Gel retardation assay

Gel retardation assay was performed as described earlier (Matera et al., 2022) with some modifications. Briefly, unlabeled *tssM* in vitro transcript (250 nt upstream and 250 nt downstream from ATG) at a fixed concentration of 20 pmol and full-length AbsR28 in vitro transcript at an increasing concentration were used for gel retardation assay. *tssM* mRNA was denatured at 65ºC for 2 min and chilled on ice for 5 min. 10X structure buffer (100 mM Tris-HCl pH 7.0 and 1 M KCl) was added at a final concentration of 1X to the mRNA and the mRNA was allowed to re-nature at 37ºC for 15 min. Yeast RNA (Ambion) was added at a final concentration of 1 µg/reaction to the reaction mix and AbsR28 was added to the tubes at an increasing concentration. $MnCl_2$ was added to all the reaction mix at a final concentration of 10 mM. After incubation at 37ºC for 60 min, 6X RNA native loading buffer (Ambion) was added to stop the reaction and resolved on a 6% native PAGE at 4ºC in 0.5% TBE at a constant current of 40 mA for 6 h. The gel was stained with SYBR Safe and visualized the RNA bands using a phosphorimager (Typhoon FLA 9000, GE Healthcare) and ImageQuant software.

RNase E-mediated degradation assay

The in vitro transcript *tssM* (250 nt upstream and 250 nt downstream from ATG) was 5'-labeled with [^{32}P]-γ-ATP as described above. 5'-labeled *tssM* mRNA (5 pmol) was denatured at 65ºC for 2 min and chilled on ice for 5 min. 10X structure buffer (100 mM Tris-HCl pH 7.0 and 1 M KCl) was added at a final concentration of 1X to the mRNA and the mRNA was allowed to re-nature at 37ºC for 15 min. Yeast RNA (Ambion) was added to the reaction mix at a final

concentration of 1 µg/reaction. Unlabeled AbsR28 (35 pmol) and purified *A. baumannii* Hfq72, or *E. coli* Hfq protein (5 fold molar excess in hexamer over *tssM*), were added to the tubes. $MnCl_2$ was added to all the reaction mix at a final concentration of 10 mM. The reaction mixture was incubated at 37ºC for 60 min. To initiate the RNase E-mediated degradation, purified RNase E (10 fold molar excess over *tssM*) was added to the reaction mixture and incubated further at 37ºC for 210 min (0 min denoted the initial time point when RNase E was added). EDTA (2.5 µL from 50 mM stock) and Proteinase K (2.5 µL from 20 mg/mL stock) were added to each reaction mixture and incubated at 50ºC for 10 min. Samples were purified immediately using 2X precipitation buffer supplied with RNase T1 kit (Ambion) according to the manufacturer's instruction. RNA pellets were dissolved in loading buffer II (Ambion) and denatured for 3 min at 95ºC. RNA cleavage products were resolved on 6% native PAGE at a constant 15 Watt. After gel drying for 2 h at 80ºC, bands were visualized using a phosphoimager (Typhoon FLA 9000, GE Healthcare) and ImageQuant software.

Mice infection model for *A. baumannii* pneumonia

Mice (n = 8 for each group, determined using G*Power analysis) were infected intranasally with *A. baumannii* and CFU was enumerated as previously described (Palmer et al., 2019) with some modification. Briefly, all the indicated strains were streaked freshly on LB-agar plates and incubated at 37ºC in shaking for O/N. One fresh colony for each strain was used to inoculate in 5 mL LB-medium and grown at 37ºC in shaking for O/N. The cultures were diluted to a 1:1000 ratio in fresh 10 mL LB-medium and 37ºC in shaking till OD_{600} 0.6 (mid-log phase). Bacterial cells were harvested by centrifugation at 6000g for 5 min at 4ºC, washed with 1 mL ice-cold 1X sterile PBS, resuspended the pellet into ice-cold 1X sterile PBS, and maintained the inoculum on ice. The mice were anesthetized and infected intranasally with 20 µL of inoculum containing 4×10^4 CFU. Mice were euthanized at 36 h of infection, and lungs and livers were harvested, immediately transferred on ice, and washed with ice-cold 1X sterile PBS. The harvested organs were chopped into pieces to enumerate bacterial burden, histopathology, qRT-PCR, Western Blot, and ICP-MS analysis. For enumeration of bacterial

784 burden in the infected organs, the weight of the organs was measured using an analytical
785 balance (G&G), homogenized using a tissue homogenizer, serially diluted into PBS, and
786 plated onto Leeds *Acinetobacter* medium plates. After incubation at 37ºC for O/N, the bacterial
787 colonies were enumerated. For histopathology, harvested organs were fixed in a natural buffer
788 solution containing formalin for fixation before embedding in paraffin blocks. Tissue sections
789 were stained with hematoxylin and eosin, and slides were visualized under a microscope
790 (Zeiss). For Western Blotting, the harvested tissue samples were homogenized in PBS
791 containing protease inhibitor cocktail (Thermo Fisher Scientific). The protein concentration
792 was determined by a BCA protein assay kit (TakaRa) using bovine serum albumin (BSA) as
793 a standard. The Western Blotting was performed as described above and around 15 µg of the
794 total protein was used for this.

795 **QUANTIFICATION AND STATISTICAL ANALYSIS**

796 Statistical analyses were performed using GraphPad Prism 8. Each figure legend clearly
797 defines the exact statistical tests, number of repeated experiments, significance values, and
798 group sizes.

799 **ACKNOWLEDGEMENTS**

800 We thank all the members of the Pathania Lab for their valuable suggestions and fruitful
801 discussions regarding this manuscript. We are grateful to Prof. S.P. Mukherjee for the training
802 required to handle [γ-^{32}P]ATP at IIT Roorkee. We extend heartfelt thanks to Prof. N.K. Navani
803 (IIT Roorkee) for his scientific inputs during experiments and critical views on the manuscript.
804 We thank Dr. Jawed Akhter and Nishant Jyoti for their help during animal experiments. We
805 are incredibly thankful to Arpita Dey for helping with the ITC assay and data analysis. We also
806 thank Prof. P. Roy (IIT Roorkee) and members of his laboratory for animal cell lines. We are
807 grateful to Institute Instrumentation Centre (IIC) in IIT Roorkee for providing facilities like ICP-
808 MS and ITC. This work was funded by DBT/Wellcome Trust India Alliance Senior Fellowship
809 (Ref. IA/S/21/1/505588) to R.P. S.B. was supported by a Research Fellow Award (Sr. No.

2061530396; Ref. No. 21/06/2015(i)EU-V) from University Grants Commission (UGC). A.P. was supported by a fellowship (Ref. No. 09/143(1019)/2020-EMR-I) from CSIR. K.D. was supported by a fellowship (Ref. No. DST/INSPIRE/03/2017/000008) from DST. The funders had no role in study design, data collection, interpretation, or the decision to submit the work for publication.

AUTHORS CONTRIBUTIONS

S.B. and R.P. designed the study, conceptualized the experiments, and interpreted data. S.B. performed the experiments and analysis. A.P. helped in gel retardation assay. K.D. purified proteins required for RNase E degradation assay. R.S. and T.K.S. provided the radioactive facility for lead acetate probing only, and S.C. helped in radio labeling AbsR28 for lead acetate probing at THSTI. R.P. engaged in funding acquisition. S.B. and R.P. wrote the manuscript, which all authors commented on.

DECLARATION OF INTERESTS

The authors declare no competing interests.

REFERENCES

1. Ahn, S., Jung, J., Jang, I.A., Madsen, E.L., and Park, W. (2016). Role of glyoxylate shunt in oxidative stress response. Journal of Biological Chemistry 291(22), pp.11928-11938.
2. Afonyushkin, T., Vecˇerek, B., Moll, I., Blasi, U., and Kaberdin, V.R. (2005). Both RNase E and RNase III control the stability of sodB mRNA upon translational inhibition by the small regulatory RNA RyhB. Nucleic Acids Research 33(5), pp.1678-1689.
3. Balasubramanian, D., and Vanderpool, C.K. (2013). New developments in post-transcriptional regulation of operons by small RNAs. RNA Biology 10(3), pp.337-341.
4. Basler, M. (2015). Type VI secretion system: secretion by a contractile nanomachine. Philosophical Transactions of the Royal Society B: Biological Sciences 370(1679), p.20150021.
5. Bergogne-Berezin, E., and Towner, K.J. (1996). *Acinetobacter* spp. as nosocomial pathogens: microbiological, clinical, and epidemiological features. Clinical Microbiology Reviews 9(2), pp.148-165.
6. Bernard, C.S., Brunet, Y.R., Gueguen, E., and Cascales, E. (2010). Nooks and crannies in type VI secretion regulation. Journal of Bacteriology 192(15), pp.3850-3860.
7. Brencic, A., and Lory, S. (2009). Determination of the regulon and identification of novel mRNA targets of *Pseudomonas aeruginosa* RsmA. Molecular Microbiology 72(3), pp.612-632.
8. Brunet, Y.R., Zoued, A., Boyer, F., Douzi, B., and Cascales, E. (2015). The type VI secretion TssEFGK-VgrG phage-like baseplate is recruited to the TssJLM membrane complex via multiple contacts and serves as assembly platform for tail tube/sheath polymerization. PLoS Genetics 11(10), p.e1005545.

9. Cao, Z., Casabona, M.G., Kneuper, H., Chalmers, J.D., and Palmer, T. (2016). The type VII secretion system of *Staphylococcus aureus* secretes a nuclease toxin that targets competitor bacteria. Nature Microbiology 2(1), pp.1-11.
10. Caron, M.P., Lafontaine, D.A., and Massé, E. (2010). Small RNA-mediated regulation at the level of transcript stability. RNA Biology 7(2), pp.140-144.
11. Cianfanelli, F.R., Monlezun, L., and Coulthurst, S.J. (2016). Aim, load, fire: the type VI secretion system, a bacterial nanoweapon. Trends in Microbiology 24(1), pp.51-62.
12. Coady, A., Xu, M., Phung, Q., Cheung, T.K., Bakalarski, C., Alexander, M.K., Lehar, S.M., Kim, J., Park, S., Tan, M.W., and Nishiyama, M. (2015). The *Staphylococcus aureus* ABC-type manganese transporter MntABC is critical for reinitiation of bacterial replication following exposure to phagocytic oxidative burst. PLoS One 10(9), p.e0138350.
13. Dambach, M., Sandoval, M., Updegrove, T.B., Anantharaman, V., Aravind, L., Waters, L.S., and Storz, G. (2015). The ubiquitous yybP-ykoY riboswitch is a manganese-responsive regulatory element. Molecular Cell 57(6), pp.1099-1109.
14. Datsenko, K.A., and Wanner, B.L. (2000). One-step inactivation of chromosomal genes in *Escherichia coli* K-12 using PCR products. Proceedings of the National Academy of Sciences 97, 6640–6645.
15. Desnoyers, G., and Massé, E. (2012). Noncanonical repression of translation initiation through small RNA recruitment of the RNA chaperone Hfq. Genes & Development 26(7), pp.726-739.
16. Dexter, C., Murray, G.L., Paulsen, I.T., and Peleg, A.Y. (2015). Community-acquired *Acinetobacter baumannii*: clinical characteristics, epidemiology and pathogenesis. Expert Review of Anti-infective Therapy 13(5), pp.567-573.
17. Falagas, M.E., Bliziotis, I.A., and Siempos, I.I. (2006). Attributable mortality of *Acinetobacter baumannii* infections in critically ill patients: a systematic review of matched cohort and case-control studies. Critical Care 10(2), pp.1-8.
18. Felisberto-Rodrigues, C., Durand, E., Aschtgen, M.S., Blangy, S., Ortiz-Lombardia, M., Douzi, B., Cambillau, C., and Cascales, E. (2011). Towards a structural comprehension of bacterial type VI secretion systems: characterization of the TssJ-TssM complex of an *Escherichia coli* pathovar. PLoS Pathogens 7(11), p.e1002386.
19. Franze de Fernandez, M.T., Eoyang, L., and August, J.T. (1968). Factor fraction required for the synthesis of bacteriophage Qβ-RNA. Nature 219(5154), pp.588-590.
20. García-Bayona, L., Guo, M.S., and Laub, M.T. (2017). Contact-dependent killing by *Caulobacter crescentus* via cell surface-associated, glycine zipper proteins. Elife 6, p.e24869.
21. Gripenland, J., Netterling, S., Loh, E., Tiensuu, T., Toledo-Arana, A., and Johansson, J. (2010). RNAs: regulators of bacterial virulence. Nature Reviews Microbiology 8(12), pp.857-866.
22. Guillier, M., and Gottesman, S. (2008). The 5′ end of two redundant sRNAs is involved in the regulation of multiple targets, including their own regulator. Nucleic Acids Research 36(21), pp.6781-6794.
23. Hassan, H.M., and Fridovich, I. (1977). Regulation of the synthesis of superoxide dismutase in *Escherichia coli*. Induction by methyl viologen. Journal of Biological Chemistry 252(21), pp.7667-7672.
24. Holmqvist, E., and Wagner, E.G.H. (2017). Impact of bacterial sRNAs in stress responses. Biochemical Society Transactions 45(6), pp.1203-1212.
25. Hood, M.I., Mortensen, B.L., Moore, J.L., Zhang, Y., Kehl-Fie, T.E., Sugitani, N., Chazin, W.J., Caprioli, R.M., and Skaar, E.P. (2012). Identification of an *Acinetobacter baumannii* zinc acquisition system that facilitates resistance to calprotectin-mediated zinc sequestration. PLoS Pathogens 8(12), p.e1003068.
26. Hood, M.I., and Skaar, E.P. (2012). Nutritional immunity: transition metals at the pathogen–host interface. Nature Reviews Microbiology 10(8), pp.525-537.
27. Hong, Y., Zeng, J., Wang, X., Drlica, K., and Zhao, X. (2019). Post-stress bacterial cell death mediated by reactive oxygen species. Proceedings of the National Academy of Sciences 116(20), pp.10064-10071.
28. Janssen, K.H., Diaz, M.R., Golden, M., Graham, J.W., Sanders, W., Wolfgang, M.C., and Yahr, T.L. (2018). Functional analyses of the RsmY and RsmZ small noncoding regulatory RNAs in *Pseudomonas aeruginosa*. Journal of Bacteriology 200(11), pp.e00736-17.

29. Juttukonda, L.J., Chazin, W.J., and Skaar, E.P. (2016). *Acinetobacter baumannii* coordinates urea metabolism with metal import to resist host-mediated metal limitation. mBio 7(5), pp.e01475-16.
30. Juttukonda, L.J., and Skaar, E.P. (2015). Manganese homeostasis and utilization in pathogenic bacteria. Molecular Microbiology 97(2), pp.216-228.
31. Kaye, K.S., and Pogue, J.M. (2015). Infections caused by resistant gram-negative bacteria: epidemiology and management. Pharmacotherapy: The Journal of Human Pharmacology and Drug Therapy 35(10), pp.949-962.
32. Kehl-Fie, T.E., Chitayat, S., Hood, M.I., Damo, S., Restrepo, N., Garcia, C., Munro, K.A., Chazin, W.J., and Skaar, E.P. (2011). Nutrient metal sequestration by calprotectin inhibits bacterial superoxide defense, enhancing neutrophil killing of *Staphylococcus aureus*. Cell Host & Microbe 10(2), pp.158-164.
33. Kehres, D.G., and Maguire, M.E. (2003). Emerging themes in manganese transport, biochemistry and pathogenesis in bacteria. FEMS Microbiology Reviews 27(2-3), pp.263-290.
34. Lin, J., Zhang, W., Cheng, J., Yang, X., Zhu, K., Wang, Y., Wei, G., Qian, P.Y., Luo, Z.Q., and Shen, X. (2017). A *Pseudomonas* T6SS effector recruits PQS-containing outer membrane vesicles for iron acquisition. Nature Communications 8(1), pp.1-12.
35. Livak, K.J., and Schmittgen, T.D. (2001). Analysis of relative gene expression data using real -time quantitative PCR and the 2 -ΔΔCT method. Methods 25, 402–408.
36. Lopez, J., Ly, P.M., and Feldman, M.F. (2020). The tip of the VgrG spike is essential to functional type VI secretion system assembly in *Acinetobacter baumannii*. mBio 11(1), pp.e02761-19.
37. Ma, L.S., Narberhaus, F., and Lai, E.M. (2012). IcmF family protein TssM exhibits ATPase activity and energizes type VI secretion. Journal of Biological Chemistry 287(19), pp.15610-15621.
38. Marden, J.N., Diaz, M.R., Walton, W.G., Gode, C.J., Betts, L., Urbanowski, M.L., Redinbo, M.R., Yahr, T.L., and Wolfgang, M.C. (2013). An unusual CsrA family member operates in series with RsmA to amplify posttranscriptional responses in *Pseudomonas aeruginosa*. Proceedings of the National Academy of Sciences 110(37), pp.15055-15060.
39. Matera, G., Altuvia, Y., Gerovac, M., El Mouali, Y., Margalit, H., and Vogel, J. (2022). Global RNA interactome of *Salmonella* discovers a 5′ UTR sponge for the MicF small RNA that connects membrane permeability to transport capacity. Molecular Cell 82(3), pp.629-644.
40. Meumann, E.M., Anstey, N.M., Currie, B.J., Piera, K.A., Kenyon, J.J., Hall, R.M., Davis, J.S., and Sarovich, D.S. (2019). Genomic epidemiology of severe community-onset *Acinetobacter baumannii* infection. Microbial Genomics 5(3).
41. Monteith, A.J., and Skaar, E.P. (2021). The impact of metal availability on immune function during infection. Trends in Endocrinology & Metabolism 32(11), pp.916-928.
42. Morita, T., Maki, K., and Aiba, H. (2005). RNase E-based ribonucleoprotein complexes: mechanical basis of mRNA destabilization mediated by bacterial noncoding RNAs. Genes & Development 19(18), pp.2176-2186.
43. Mortensen, B.L., and Skaar, E.P. (2013). The contribution of nutrient metal acquisition and metabolism to *Acinetobacter baumannii* survival within the host. Frontiers in Cellular and Infection Microbiology 3, p.95.
44. Mougous, J.D., Cuff, M.E., Raunser, S., Shen, A., Zhou, M., Gifford, C.A., Goodman, A.L., Joachimiak, G., Ordoñez, C.L., Lory, S., and Walz, T. (2006). A virulence locus of *Pseudomonas aeruginosa* encodes a protein secretion apparatus. Science 312(5779), pp.1526-1530.
45. Munoz-Price, L.S., Zembower, T., Penugonda, S., Schreckenberger, P., Lavin, M.A., Welbel, S., Vais, D., Baig, M., Mohapatra, S., Quinn, J.P., and Weinstein, R.A. (2010). Clinical outcomes of carbapenem-resistant *Acinetobacter baumannii* bloodstream infections: study of a 2-state monoclonal outbreak. Infection Control & Hospital Epidemiology 31(10), pp.1057-1062.
46. Murdoch, C.C., and Skaar, E.P. (2022). Nutritional immunity: the battle for nutrient metals at the host–pathogen interface. Nature Reviews Microbiology pp.1-14.
47. Palmer, L. D., Green, E. R., Sheldon, J. R., and Skaar, E. P. (2019). Assessing *Acinetobacter baumannii* virulence and persistence in a murine model of lung infection. Methods in Molecular Biology 1946, 289-305.
48. Peleg, A.Y., Seifert, H., and Paterson, D.L. (2008). *Acinetobacter baumannii*: emergence of a successful pathogen. Clinical Microbiology Reviews 21(3), pp.538-582.
49. Porcheron, G., Garénaux, A., Proulx, J., Sabri, M., and Dozois, C.M. (2013). Iron, copper, zinc, and manganese transport and regulation in pathogenic *Enterobacteria*: correlations between strains, site

of infection and the relative importance of the different metal transport systems for virulence. Frontiers in Cellular and Infection Microbiology 3, p.90.

50. Prévost, K., Desnoyers, G., Jacques, J.F., Lavoie, F., and Massé, E. (2011). Small RNA-induced mRNA degradation achieved through both translation block and activated cleavage. Genes & Development 25(4), pp.385-396.
51. Price, I.R., Gaballa, A., Ding, F., Helmann, J.D., and Ke, A., (2015). Mn2+-sensing mechanisms of yybP-ykoY orphan riboswitches. Molecular cell 57(6), pp.1110-1123.
52. Repizo, G.D., Gagné, S., Foucault-Grunenwald, M.L., Borges, V., Charpentier, X., Limansky, A.S., Gomes, J.P., Viale, A.M., and Salcedo, S.P. (2015). Differential role of the T6SS in *Acinetobacter baumannii* virulence. PloS One 10(9), p.e0138265.
53. Romby, P., Vandenesch, F., and Wagner, E.G.H. (2006). The role of RNAs in the regulation of virulence-gene expression. Current Opinion in Microbiology 9(2), pp.229-236.
54. Romero, M., Silistre, H., Lovelock, L., Wright, V.J., Chan, K.G., Hong, K.W., Williams, P., Cámara, M., and Heeb, S. (2018). Genome-wide mapping of the RNA targets of the *Pseudomonas aeruginosa* riboregulatory protein RsmN. Nucleic Acids Research 46(13), pp.6823-6840.
55. Schieber, M., and Chandel, N.S. (2014). ROS function in redox signaling and oxidative stress. Current Biology 24(10), pp.R453-R462.
56. Schuppli, D., Georgijevic, J., and Weber, H. (2000). Synergism of mutations in bacteriophage Qβ RNA affecting host factor dependence of Qβ replicase. Journal of Molecular Biology 295(2), pp.149-154.
57. Sharma, R., Arya, S., Patil, S.D., Sharma, A., Jain, P.K., Navani, N.K., and Pathania, R. (2014). Identification of novel regulatory small RNAs in *Acinetobacter baumannii*. PloS One 9(4), p.e93833.
58. Si, M., Wang, Y., Zhang, B., Zhao, C., Kang, Y., Bai, H., Wei, D., Zhu, L., Zhang, L., Dong, T.G., and Shen, X. (2017a). The type VI secretion system engages a redox-regulated dual-functional heme transporter for zinc acquisition. Cell Reports 20(4), pp.949-959.
59. Si, M., Zhao, C., Burkinshaw, B., Zhang, B., Wei, D., Wang, Y., Dong, T.G., and Shen, X. (2017b). Manganese scavenging and oxidative stress response mediated by type VI secretion system in *Burkholderia thailandensis*. Proceedings of the National Academy of Sciences 114(11), pp.E2233-E2242.
60. Silverman, J.M., Brunet, Y.R., Cascales, E., and Mougous, J.D. (2012). Structure and regulation of the type VI secretion system. Annual Review of Microbiology 66, p.453.
61. Souza, D.P., Oka, G.U., Alvarez-Martinez, C.E., Bisson-Filho, A.W., Dunger, G., Hobeika, L., Cavalcante, N.S., Alegria, M.C., Barbosa, L.R., Salinas, R.K., and Guzzo, C.R. (2015). Bacterial killing via a type IV secretion system. Nature Communications 6(1), pp.1-9.
62. Stietz, M.S., Liang, X., Li, H., Zhang, X., and Dong, T.G. (2020). TssA–TssM–TagA interaction modulates type VI secretion system sheath-tube assembly in *Vibrio cholerae*. Nature Communications 11(1), pp.1-11.
63. Traglia, G., Chiem, K., Quinn, B., Fernandez, J.S., Montaña, S., Almuzara, M., Mussi, M.A., Tolmasky, M.E., Iriarte, A., Centrón, D., and Ramírez, M.S. (2018). Genome sequence analysis of an extensively drug-resistant *Acinetobacter baumannii* indigo-pigmented strain depicts evidence of increase genome plasticity. Scientific Reports 8(1), pp.1-15.
64. Tucker, A.T., Nowicki, E.M., Boll, J.M., Knauf, G.A., Burdis, N.C., Trent, M.S., and Davies, B.W. (2014). Defining gene-phenotype relationships in *Acinetobacter baumannii* through one-step chromosomal gene inactivation. mBio 5(4), pp.e01313-14.
65. Urban, J.H., and Vogel, J. (2007). Translational control and target recognition by *Escherichia coli* small RNAs in vivo. Nucleic Acids Research 35(3), pp.1018-1037.
66. VanRheenen, S.M., Duménil, G., and Isberg, R.R. (2004). IcmF and DotU are required for optimal effector translocation and trafficking of the *Legionella pneumophila* vacuole. Infection and Immunity 72(10), pp.5972-5982.
67. Vassallo, C.N., Cao, P., Conklin, A., Finkelstein, H., Hayes, C.S., and Wall, D. (2017). Infectious polymorphic toxins delivered by outer membrane exchange discriminate kin in myxobacteria. Elife 6, p.e29397.
68. Vogel, J., and Luisi, B.F. (2011). Hfq and its constellation of RNA. Nature Reviews Microbiology 9(8), pp.578-589.

69. Weber, B.S., Ly, P.M., Irwin, J.N., Pukatzki, S., and Feldman, M.F. (2015). A multidrug resistance plasmid contains the molecular switch for type VI secretion in *Acinetobacter baumannii*. Proceedings of the National Academy of Sciences 112(30), pp.9442-9447.
70. Weber, B.S., Miyata, S.T., Iwashkiw, J.A., Mortensen, B.L., Skaar, E.P., Pukatzki, S., and Feldman, M.F. (2013). Genomic and functional analysis of the type VI secretion system in *Acinetobacter*. PloS One 8(1), p.e55142.
71. Weinberg, E.D. (1975). Nutritional immunity: host's attempt to withhold iron from microbial invaders. Jama 231(1), pp.39-41.
72. Wright, M.S., Haft, D.H., Harkins, D.M., Perez, F., Hujer, K.M., Bajaksouzian, S., Benard, M.F., Jacobs, M.R., Bonomo, R.A., and Adams, M.D. (2014). New insights into dissemination and variation of the health care-associated pathogen *Acinetobacter baumannii* from genomic analysis. mBio 5(1), pp.e00963-13.
73. Zheng, J., Shin, O.S., Cameron, D.E., and Mekalanos, J.J. (2010). Quorum sensing and a global regulator TsrA control expression of type VI secretion and virulence in *Vibrio cholerae*. Proceedings of the National Academy of Sciences 107(49), pp.21128-21133.
74. Zimbler, D.L., Arivett, B.A., Beckett, A.C., Menke, S.M., and Actis, L.A. (2013). Functional features of TonB energy transduction systems of *Acinetobacter baumannii*. Infection and Immunity 81(9), pp.3382-3394.

MAIN FIGURE LEGENDS

Figure 1. *A. baumannii* T6+ cells are defective in Mn^{2+}-uptake and unable to cope with oxidative stress.

(A) Bacterial strains were co-incubated with the phagocytic cell for 4 h at an MOI of 1:1. The percentage of bacterial survival was enumerated by accounting for respective untreated control (without phagocytic cell) as 100%. The data represents the mean of four independent experiments each in biological triplicates ± SEM. See also Figure S1B.

(B) Growth of the indicated strains in the presence or absence of MV (250 µM) in LB broth. The data represents the mean of four biological replicates each in technical triplicates ± SD.

(C) Bacterial intracellular ROS generation was determined by measuring the fluorescence of 2',7'-dichlorofluorescein (DCF). The data represents the mean of four biological replicates ± SD.

(D) Neutrophils were co-incubated with WT T6- and WT T6+ cells and the expression of *mntH*, *znuB*, and *tonB* transcripts in the bacterial cells was determined by qRT-PCR. The data represents the mean of three independent experiments each in technical triplicates ± SEM.

(E) Intracellular ^{55}Mn was quantified by ICP-MS. The data represents the mean of three biological replicates ± SD. See also Figure S1C.

(F) Growth of the indicated strains in the presence of MV (150 µM) alone or supplemented with either $MnCl_2$, $ZnSO_4$, or $FeCl_3$ in LB broth. The data represents the mean of three biological replicates ± SD. See also Figure S1D and S1E.

Statistical significance was determined using a multiple comparison two-way ANOVA test with the Sidak correction for multiple comparisons comparing the means of each group to one another (A & E) and Student's t-test (B, C, & D). ** denotes p-value <0.01, *** denotes p-value <0.001, **** denotes p-value <0.0001, ns denotes not significant.

Figure 2. Deletion of *mntH* exhibited a significant increase in *hcp* expression under oxidative stress.

(A) A schematic representation of T6SS (upper panel) and a schematic layout of the T6SS gene cluster in *A. baumannii* ATCC 17978 (lower panel).

(B) Transcription of *hcp* was determined by qRT-PCR. The data represents the mean of three independent experiments each in technical triplicates ± SEM. Statistical significance was determined using Student's t-test. * denotes p-value <0.05.

(C) The Hcp secretion profile of the indicated strains was confirmed by Western blot of cell lysate (CL) and culture supernatants (S). Purified His_6-Hcp was used as a positive control. Hfq was used as a loading control for CL. The data represents three independent experiments where the samples were run on one gel. See also Figure S3A.

(D) T6SS competition assay in which prey cells were subjected to killing by incubation with WT T6-, WT T6+, Δ*mntH*, and Δ*tssM* strains. The survival percentage of prey cells was enumerated by accounting respective untreated control (without predator/killer cells) as 100%. The data represents the mean of three biological replicates ± SD. Statistical significance was determined using two-way ANOVA with Tukey's multiple comparison test for each sample with the same prey killed by the killer strains. **** denotes p-value <0.0001.

(E) Recovery of surviving prey cells after co-incubation with WT T6- or Δ*mntH*.

(F) GFP fluorescence of *E. coli*-pNYL GFP was measured after co-incubation with WT T6- or Δ*mntH* at the indicated time points. The data represents the mean of six biological replicates ± SEM.

(G) Detection of Hcp secretion from individual colonies of WT T6-, and Δ*mntH* strains by Hcp-ELISA. * indicates wells with purified His_6-Hcp, used as a positive control for Hcp-ELISA. See also Figure S3B.

Figure 3. AbsR28 represses the T6SS in *A. baumannii* under oxidative stress, and Mn^{2+} is required for this regulation.

(A) The expression of several sRNAs and *hfq* was examined by qRT-PCR. The data represents the mean of three independent experiments each in technical triplicates ± SEM.

(B) RNA-seq analysis comparing RNA from MV and $MnCl_2$ (250 μM) treated ΔAbsR28 to a WT T6- control. A dotted black line denotes $p < 0.05$.

(C) Transcription of each T6SS structural gene in WT T6- and ΔAbsR28 cells was determined by qRT-PCR. The data represents the mean of three independent experiments, each in technical triplicates ± SEM.

(D) Transcription of *hcp* was determined by qRT-PCR. The data represents the mean of three independent experiments each in technical triplicates ± SEM.

(E) The Hcp secretion profile of the bacterial strains was tested by Western blot of cell lysate (CL). The data represents two independent experiments where the samples were run on one gel. See also Figure S5A.

(F) T6SS competition assay in which *E. coli* J53 prey cells were subjected to killing by ΔAbsR28-pWBAD30AbsR28 and ΔAbsR28-pWBAD30 strains. The data represents the mean of three biological replicates ± SD.

(G) Isothermal titration calorimetry (ITC) of Mn^{2+} to AbsR28. See also Figure S5B.

(H) Lead acetate probing of the 5'end-labeled [γ-^{32}P]ATP AbsR28 in increasing concentration of $MnCl_2$ provided in structure buffer. Lanes indicated as T1 and OH ladders were obtained from the same labeled AbsR28 after incubation with RNase T1 and hydroxyl anions, respectively. RNase T1 digestion was performed in duplicates at both 0.1 and 1.0 U concentrations. The position of cleaved G residues is marked at the left of the gel. See also Figure S5C.

(I) Secondary structure of *A. baumannii* AbsR28 sRNA predicted by Rfam software.

Statistical significance was determined using the multiple comparison two-way ANOVA test with the Sidak correction for multiple comparisons comparing the means of each group to one another (A, D, & F) and Student's t-test (C). * denotes p-value <0.05, ** denotes p-value <0.01, *** denotes p-value <0.001, **** denotes <0.0001, ns denotes not significant.

Figure 4. Mn^{2+} is required for AbsR28 to base-pair with *tssM* mRNA and repress the T6SS by potentiating RNase E mediated degradation of *tssM* mRNA.

(A) Predicted base-pairing between *tssM* and AbsR28 by the CopraRNA bioinformatics tool.

(B-C) Gel retardation assay of unlabeled *tssM* in vitro transcript and unlabeled full-length AbsR28 in vitro transcript in structure buffer containing either $MnCl_2$ or $MgCl_2$. See also Figure S6A and S6B.

(D) Quantification of unbound *tssM* obtained from Figures C and D are shown (n = 2 independent experiments) using ImageJ software.

(E) Transcription of *tssM* was determined after adding Rifampicin (400 µg/mL) by qRT-PCR and plotted as the fold change relative to 0 min for each sample. The data represents the mean of technical triplicates ± SD. Statistical significance was determined using the one-way ANOVA test with Dunnett's multiple comparison test. **** denotes p-value <0.0001, ns denotes not significant.

(F) Cleavage of the 5'end-labeled [γ-^{32}P]ATP *tssM* in vitro transcript was assessed by incubating with RNase E in the presence or absence of unlabeled AbsR28 and/or *A. baumannii* Hfq72 or *E. coli* Hfq protein for 0 and 3.3 hours. The complete 5'-labeled *tssM* transcripts that remain after RNase E mediated cleavage are denoted by a filled triangle.

Figure 5. Mn^{2+}-dependent AbsR28 mediated T6SS repression is required for *A. baumannii* pathogenesis.

(A) Bacterial strains were co-incubated with neutrophils for 4 h at an MOI of 1:1. Percentage of bacterial survival was enumerated, accounting for respective untreated control (without

neutrophil) as 100%. The data represents the mean of three independent experiments each in biological triplicates ± SEM.

(B) Enumeration of bacterial burden recovered from mice lungs and liver (n = 8) infected with WT T6-, WT T6+, Δ*mntH*, or ΔAbsR28 strains at 36 hpi. Data represents mean ± SD.

(C) Histopathology of the mice lungs (H&E stained) infected with WT T6-, WT T6+, Δ*mntH*, or ΔAbsR28 strains at 36 hpi. Tissue infiltration is indicated by necrosis (arrowheads) and alveolar inflammation (asterisks). The scale bar is 100 µM.

Statistical significance was determined using the one-way ANOVA test with Tukey's multiple comparisons (A & B). * denotes p-value <0.05, *** denotes p-value <0.001, ns denotes not significant.

Figure 6. Proposed model of AbsR28-mediated post-transcriptional repression of T6SS in *A. baumannii* during oxidative stress.

During oxidative stress, *A. baumannii* cells utilize MntH to increase uptake of Mn^{2+}. An elevated level of Mn^{2+} binds and alters the native structure of AbsR28 sRNA, which results in AbsR28-*tssM* mRNA complementary base-paring. The consequence of the AbsR28-*tssM* mRNA complex formation is the degradation of *tssM* by RNase E and causes repression of T6SS.

MAIN FIGURES

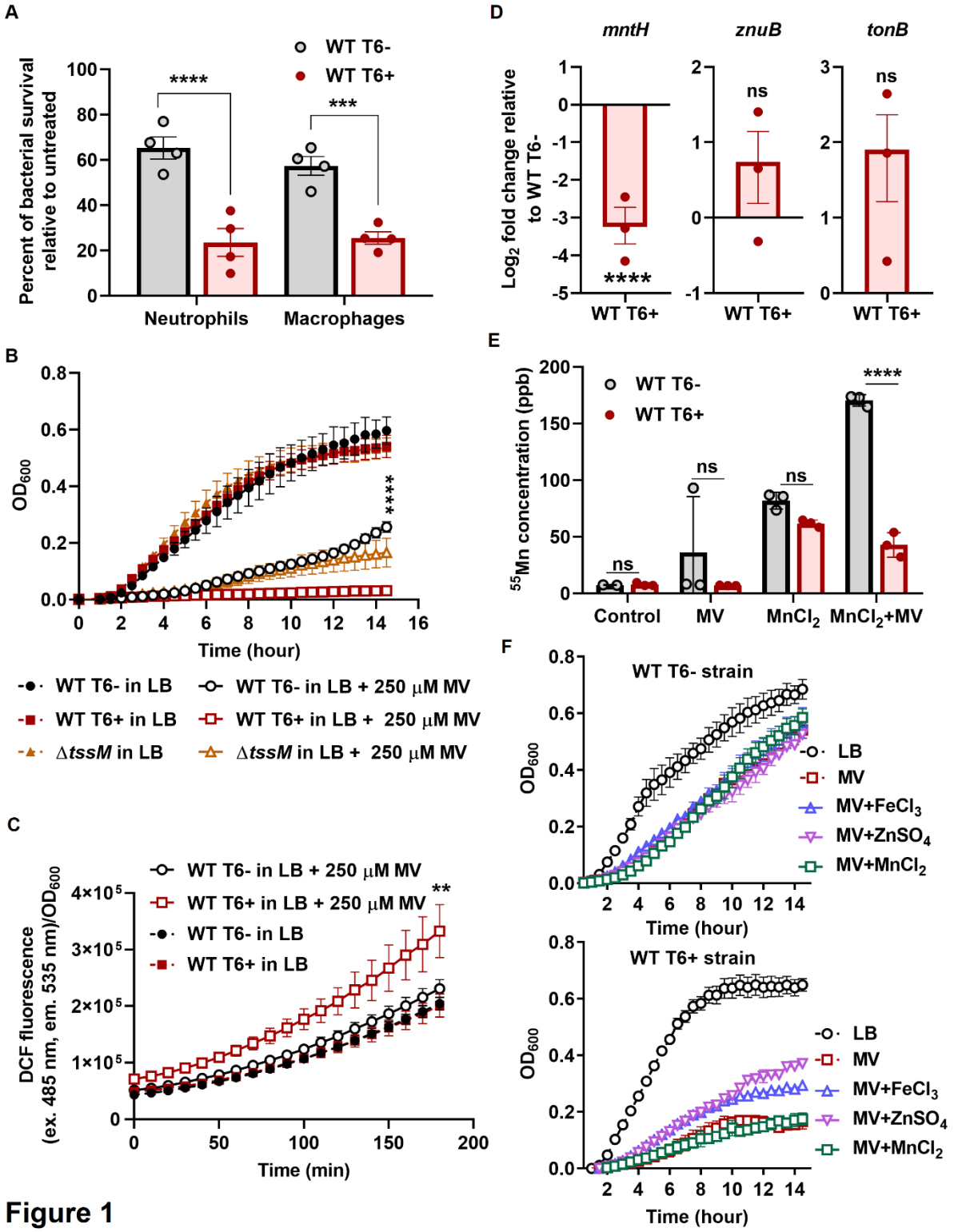

Figure 1

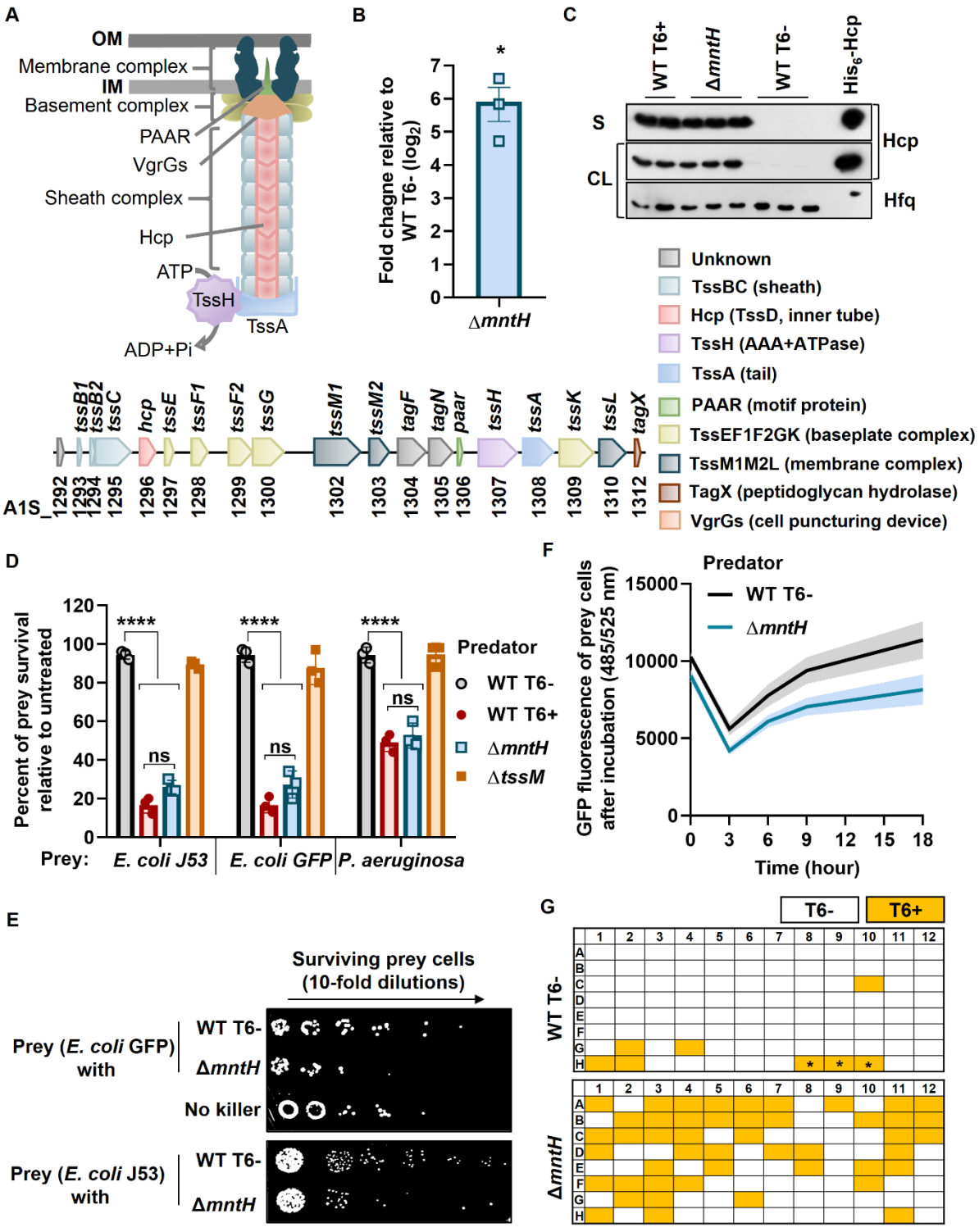

Figure 2

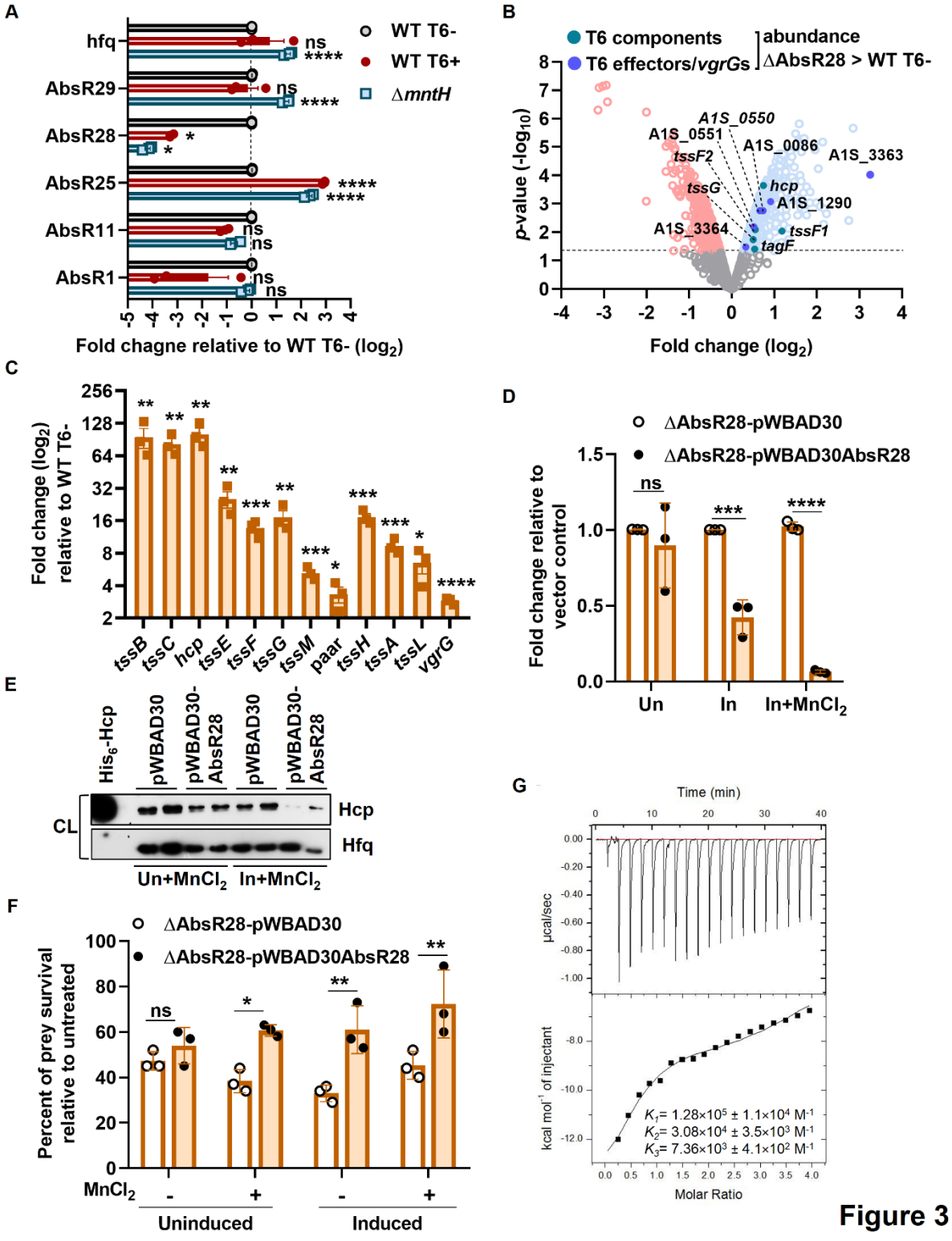

Figure 3

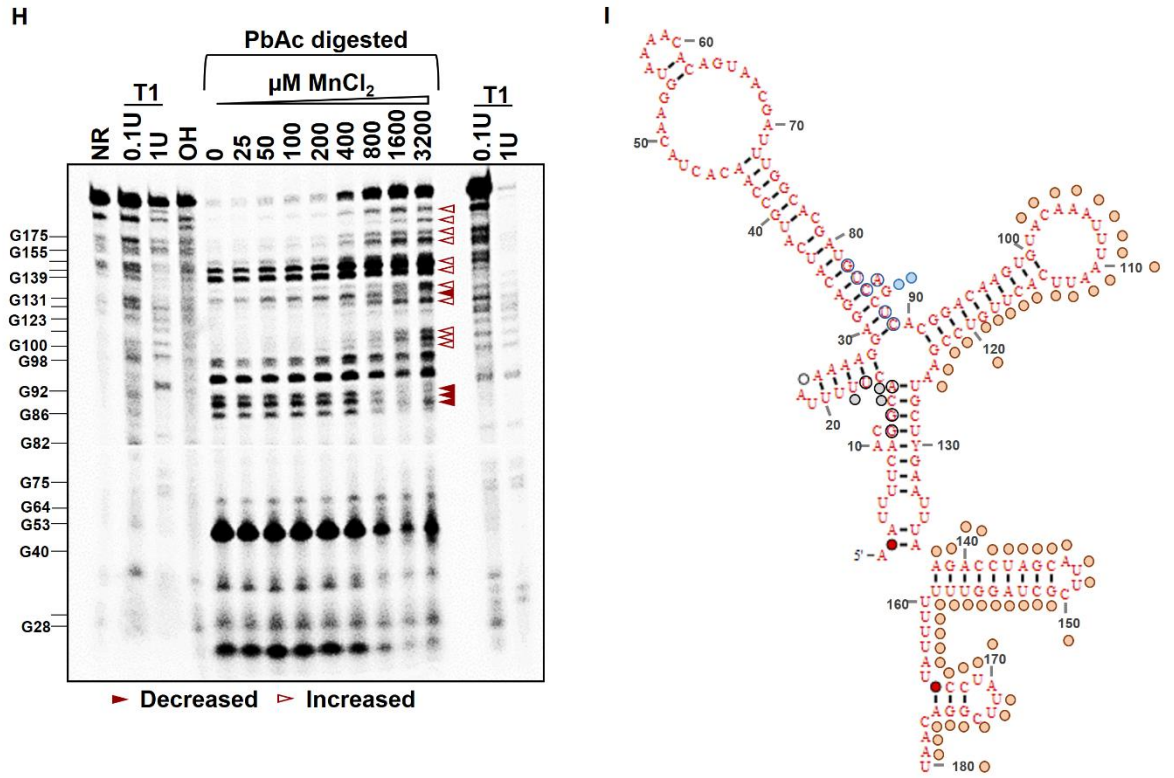

Figure 3

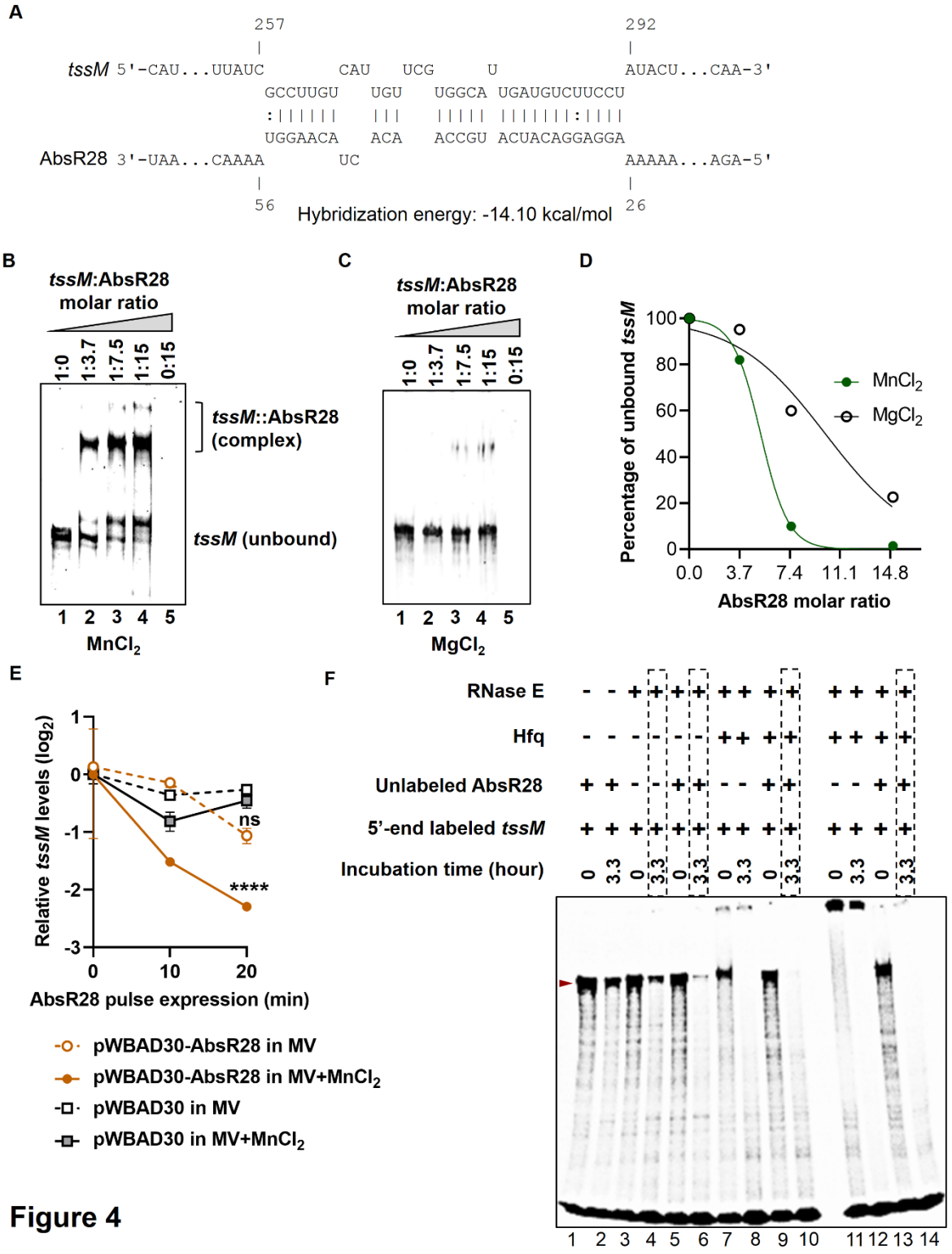

Figure 4

1169

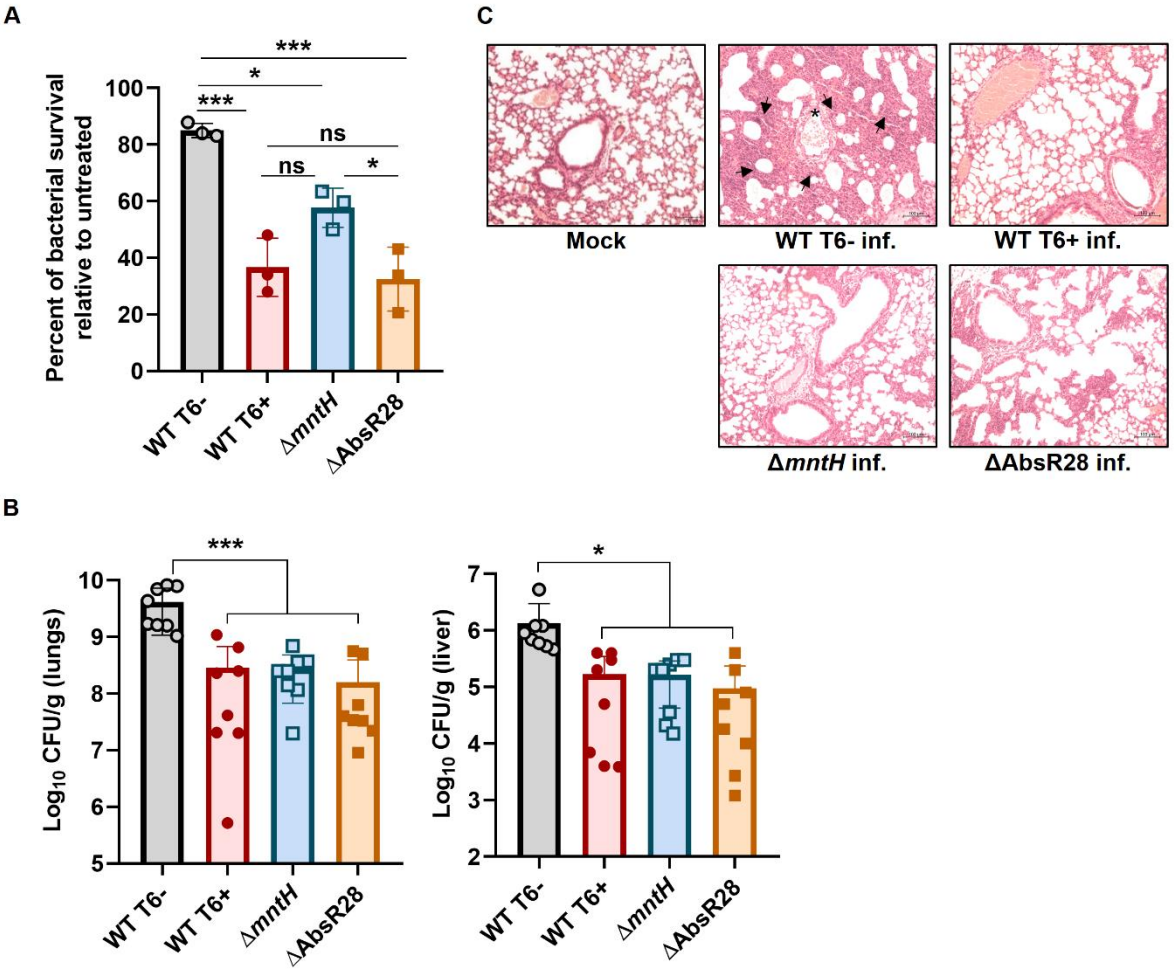

1170 **Figure 5**

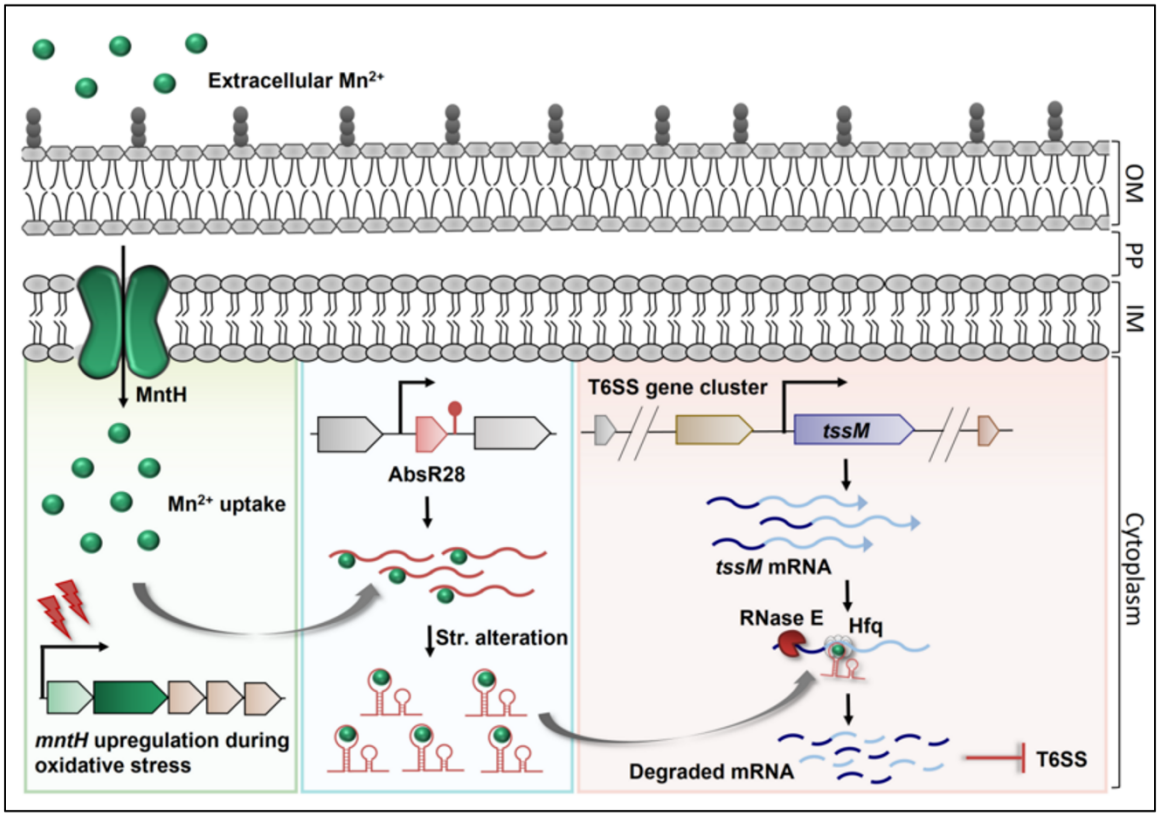

Figure 6

SUPPLEMENTARY FIGURE LEGENDS

Figure S1: *A. baumannii* T6+ cells are sensitive to oxidative stress due to inadequate Mn^{2+}-uptake. Related to Figure 1. (A) Hcp secretion profiles of the isolated WT T6- and WT T6+ strains were confirmed by Western blot. Purified His_6-Hcp was used as a positive control for Western Blot. **(B)** *A. baumannii* ATCC 17978 wild-type T6SS- (WT T6-) and wild-type T6SS+ (WT T6+) strains were co-incubated with human blood-derived neutrophils for 4 h at an MOI of 1:1. The cells were washed after incubation with gentamycin (300 µg/mL) for 2 h and neutrophils were lysed using 0.04% Triton X-100. Cell lysates were serially diluted and spotted onto LB agar plates. The untreated bacterial cells (without neutrophils) were also spotted on LB agar plates. After incubation at 37ºC overnight (O/N), the images were captured using a gel documentation system (Biorad). **(C)** Intracellular ^{66}Zn and ^{56}Fe were quantified by ICP-MS. WT T6- and WT T6+ cells were grown in minimal media (M9-media) containing Casamino acid as a nutrient source supplemented with methyl viologen (MV) and either $ZnSO_4$ or $FeCl_3$ (at a final concentration of 100 µM), and the intracellular Zn^{2+} and $Fe^{2+/3+}$ concentrations were measured in cell pellets by ICP-MS. The data represent three biological replicates with a standard deviation (SD) of the mean. Statistical significance was determined using the multiple comparison two-way ANOVA test with the Sidak correction for multiple comparisons comparing the means of each group to one another. ns denotes not significant. **(D & E)** The WT T6- and WT T6+ strains were grown in M9-media containing Casamino acid supplemented with either $MnCl_2$, $ZnSO_4$, $FeCl_3$, or altogether (250 µM each) till the mid-log phase (OD_{600}~0.6) and incubated further with MV (250 µM) or H_2O_2 (500 µM) for 2 h. Cells were washed and spotted on LB-agar plate supplemented with MV (100 µM) or H_2O_2 (500 µM) alone. After incubation at 37ºC overnight (O/N), the images were captured using a gel documentation system (Biorad).

Figure S2: pAB3 has no role in mitigating oxidative stress. Related to Figure 1. (A) The presence of both *tetR1* and *tetR2* (present in pAB3) and *hcp* in the genome of the indicated strains were confirmed by PCR. **(B)** pAB3 was transformed into the WT T6+ competent cells

and the transformants were confirmed by streaking on LB agar plate containing sulfamethoxazole/trimethoprim (S&T; 30 µg/mL and 5 µg/mL, respectively), where the cells that do not have pAB3 will not grow. **(C)** Growth of WT T6-, WT T6+, and WT T6+-pAB3 cells in LB supplemented with MV (at a final concentration of 150 µM). The data represent four biological replicates in technical triplicate with a standard deviation (SD) of the mean.

Figure S3. Deletion of *mntH* leads to an increase in T6SS expression in *A. baumannii* under oxidative stress. Related to Figure 2. (A) Uncropped Western blot images. Black boxes indicate the area included in Figure 2C. **(B)** Original pictures are captured by a camera that is schematically represented in Figure 2G.

Figure S4. AbsR28 is conserved amongst *Acinetobacter* sp., and deletion of AbsR28 has no polar effect. Related to Figure 3. (A) Distribution of AbsR28 sRNA homologs among *Acinetobacter* sp. GLASSgo software was used to find the sRNA homologs. The phylogenetic tree was generated using the Mega version X and visualized in iTol. **(B)** Genomic location of AbsR28 in *A. baumannii* ATCC 17978 (NCBI Ref. seq. CP000521.1). **(C)** To check the polar effect, WT and ΔAbsR28 strains were grown in LB supplemented with $MnCl_2$ (250 µM) till the mid-log phase (OD_{600}~0.6) and incubated further with MV (250 µM) for 2 h. RNA was extracted from the cells and cDNA was prepared. The expression of A1S_2828 and A1S_2839 transcripts, which are immediate upstream and downstream of AbsR28, respectively, was checked by qRT-PCR. No change in the expression in ΔAbsR28 for both the genes with respect to WT confirms no polar effect of ΔAbsR28.

Figure S5. AbsR28 negatively regulates T6SS in *A. baumannii* and Mn^{2+} binds to AbsR28. Related to Figure 3. (A) Uncropped Western blot images. Black boxes indicate the area included in Figure 3E. **(B)** Isothermal titration calorimetry (ITC) of Mn^{2+} to AbsR28 shows binding affinity (*K*), entropy (*ΔS*), and enthalpy (*ΔH*) of the sequential binding related to Figure 3G. (**C)** Lead acetate probing of the 5'end-labeled [γ-^{32}P]ATP AbsR28 in increasing concentration of either $MnCl_2$, $MgCl_2$, or $ZnSO_4$ provided in structure buffer. Boxes indicate bands that were altered upon increasing $MnCl_2$ concentration. Lanes indicated as T1 and OH

ladders were obtained from the same labeled AbsR28 after incubation with RNase T1 and hydroxyl anions, respectively. RNase T1 digestion was performed at both 0.1 and 1.0 U concentrations. The position of cleaved G residues is marked on the left of the gel.

Figure S6. AbsR28 base pair with *tssM* mRNA in the presence of Mn^{2+}. Related to Figure 4. (A) Complete lanes of gel retardation assay. Black boxes indicate the area included in Figures 4B and 4C.

Figure S7. The Mn^{2+}-dependent base pairing of AbsR28 and *tssM* mRNA results in T6SS repression during infection in the host. Related to Figure 5. (A) Hcp secretion profile of lung homogenates isolated from the mice (n = 3) infected with either WT T6-, WT T6+, Δ*mntH,* or ΔAbsR28 strains were confirmed by Western blot.

Figure S8. The expression of T6SS is silent in most of the tested *Acinetobacter* sp. (A) The presence of AbsR28 and *hcp* in the genome of the indicated strains was confirmed by PCR. **(B)** Hcp secretion profile of the mentioned strains grown in LB broth supplemented with MV and MnCl2 (250 µM) were confirmed by Western blot of culture supernatants. Purified His_6-Hcp was used as a positive control for Western Blot.

SUPPLEMENTARY FIGURES

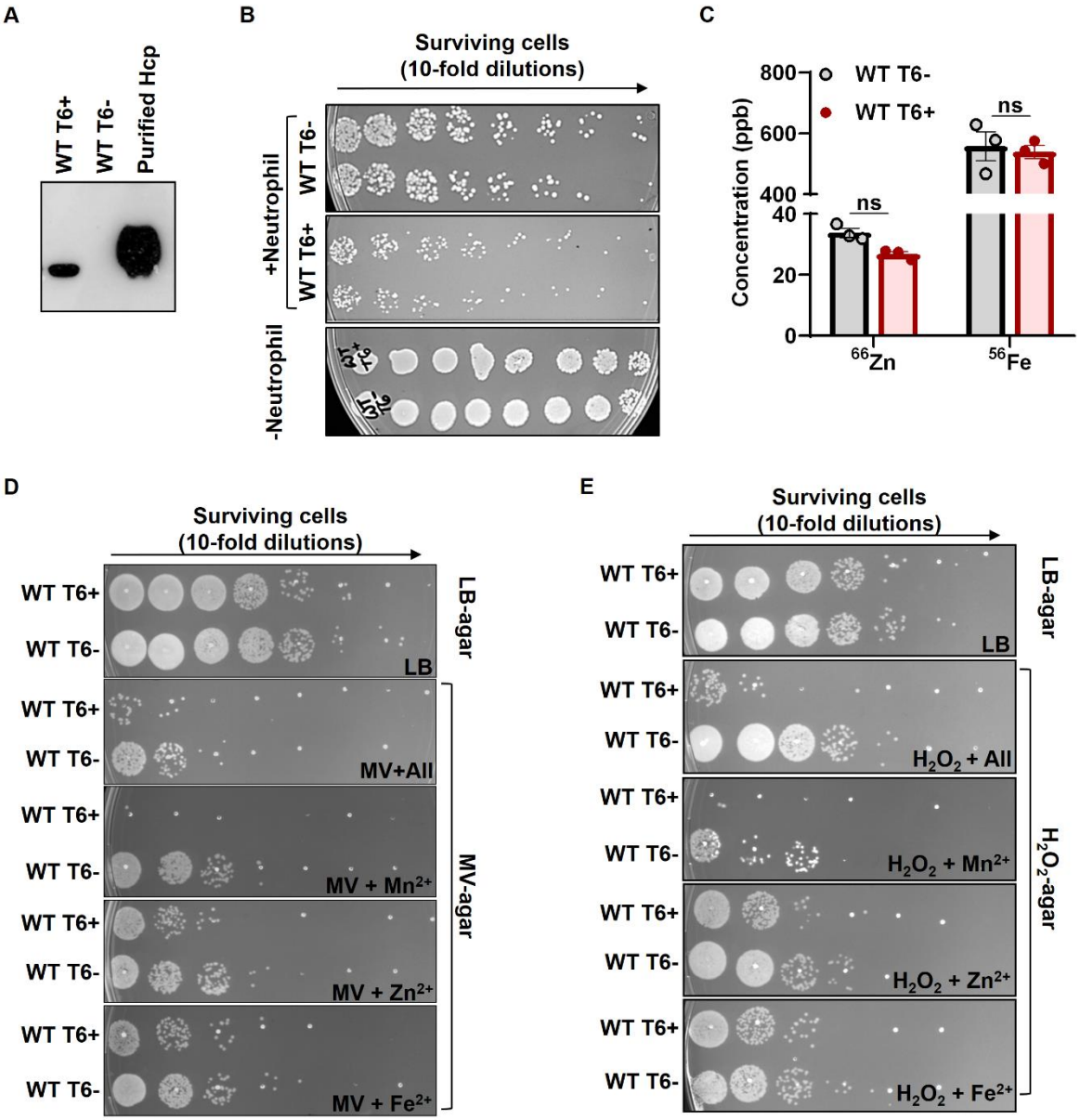

Figure S1

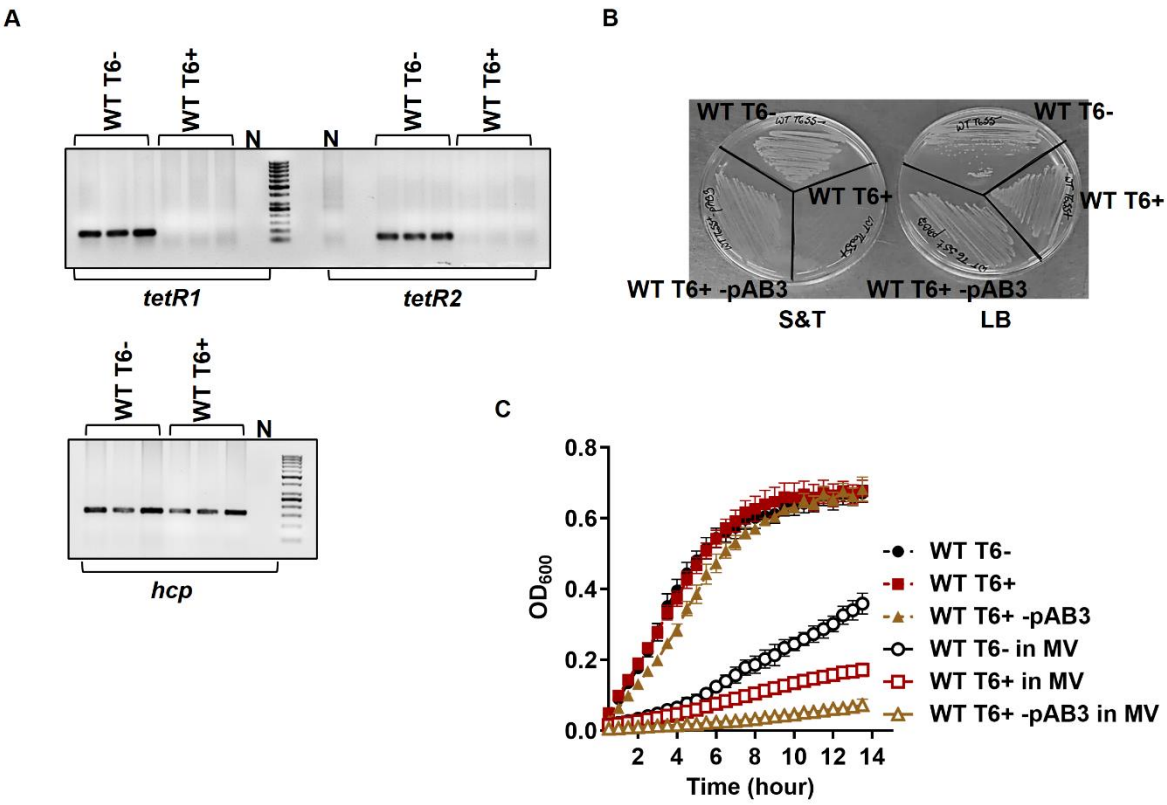

1255 **Figure S2**

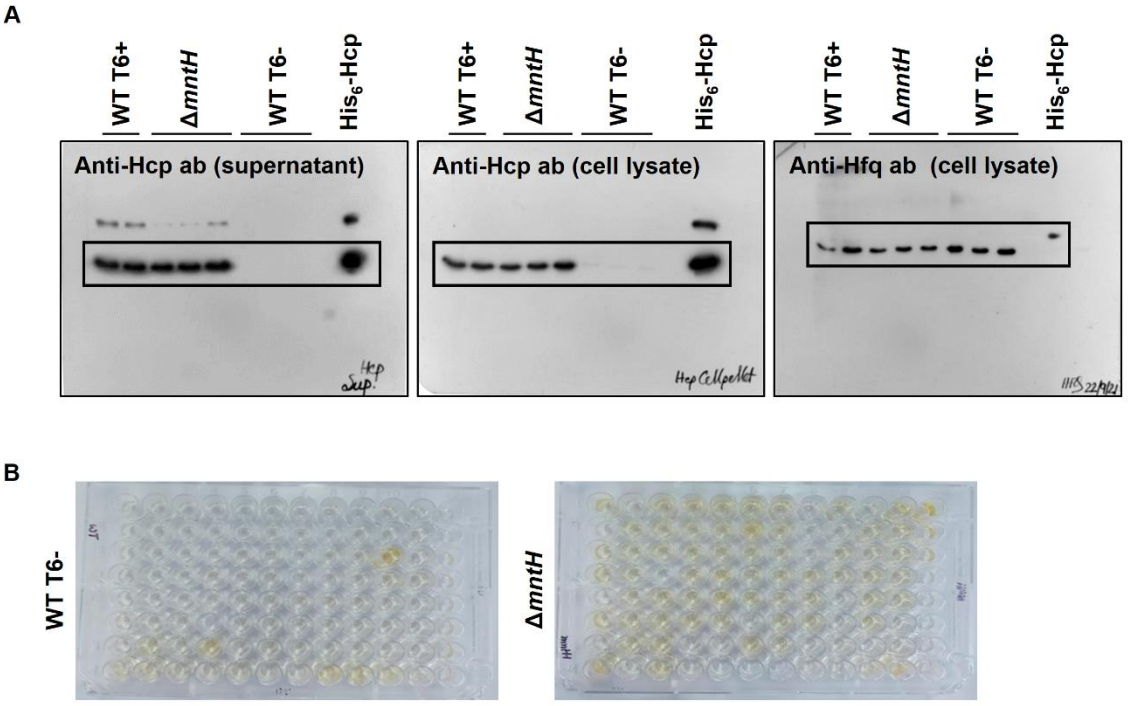

Figure S3

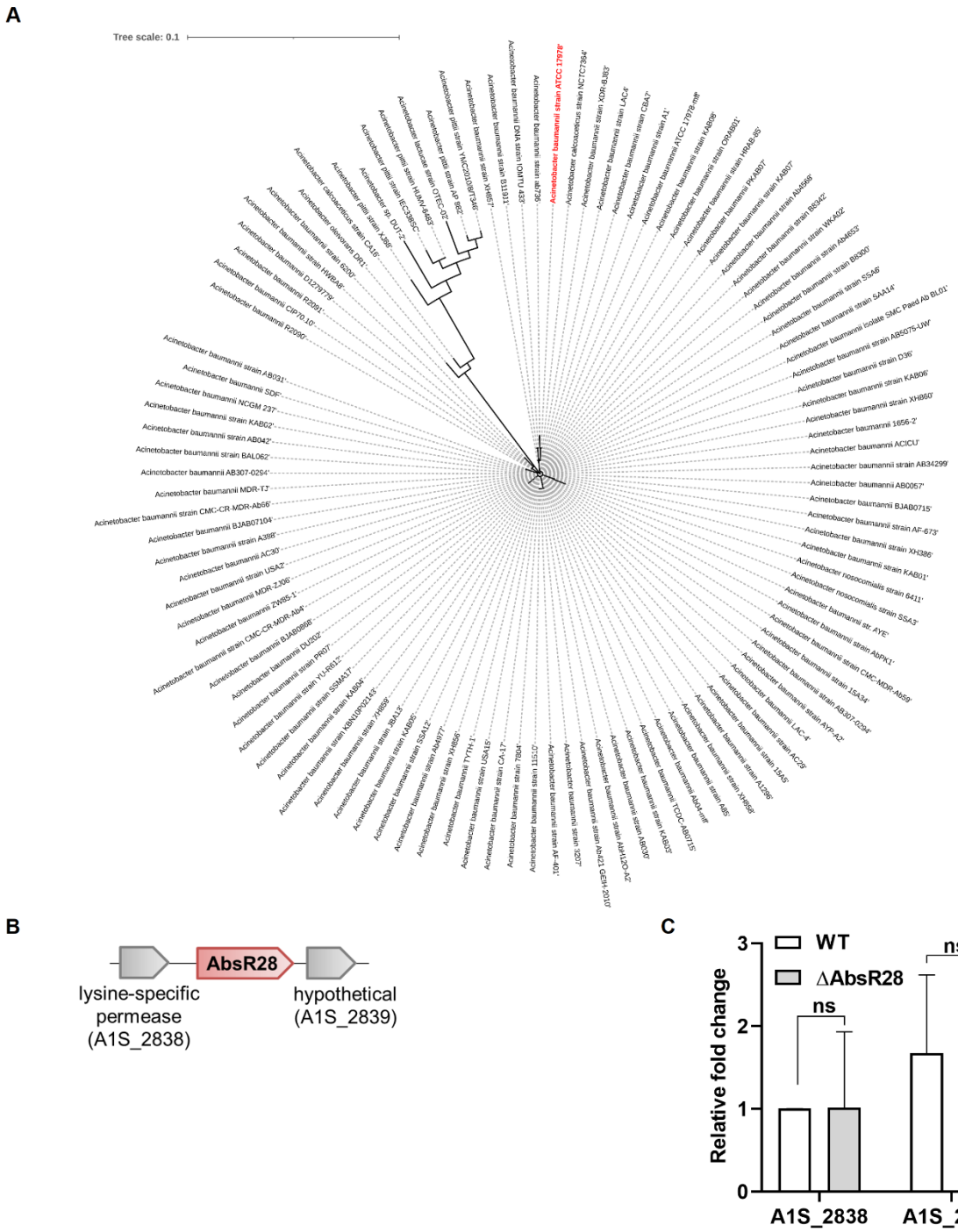

1258 **Figure S4**

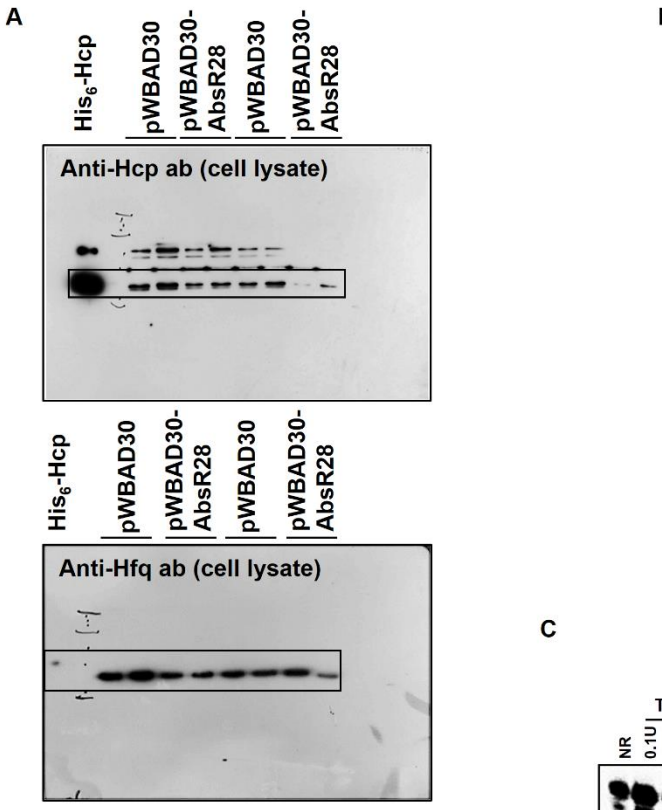

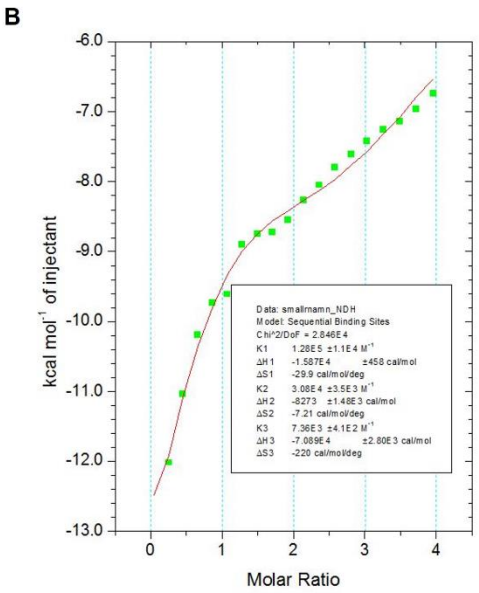

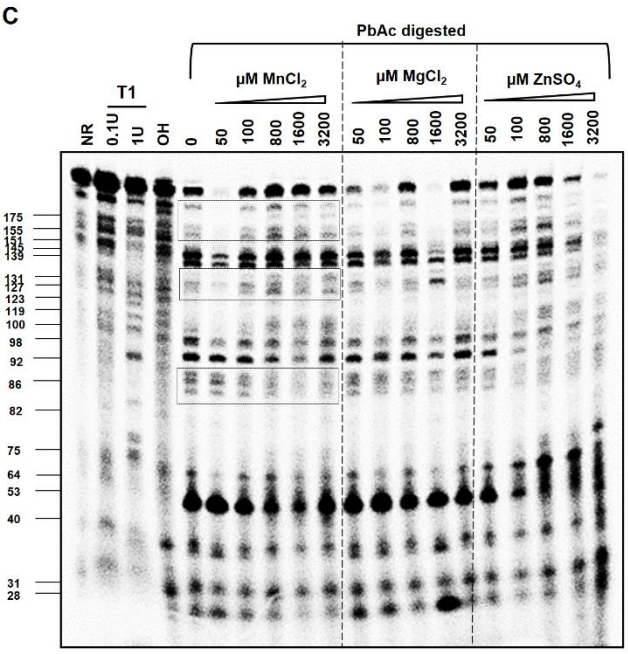

1259 **Figure S5**

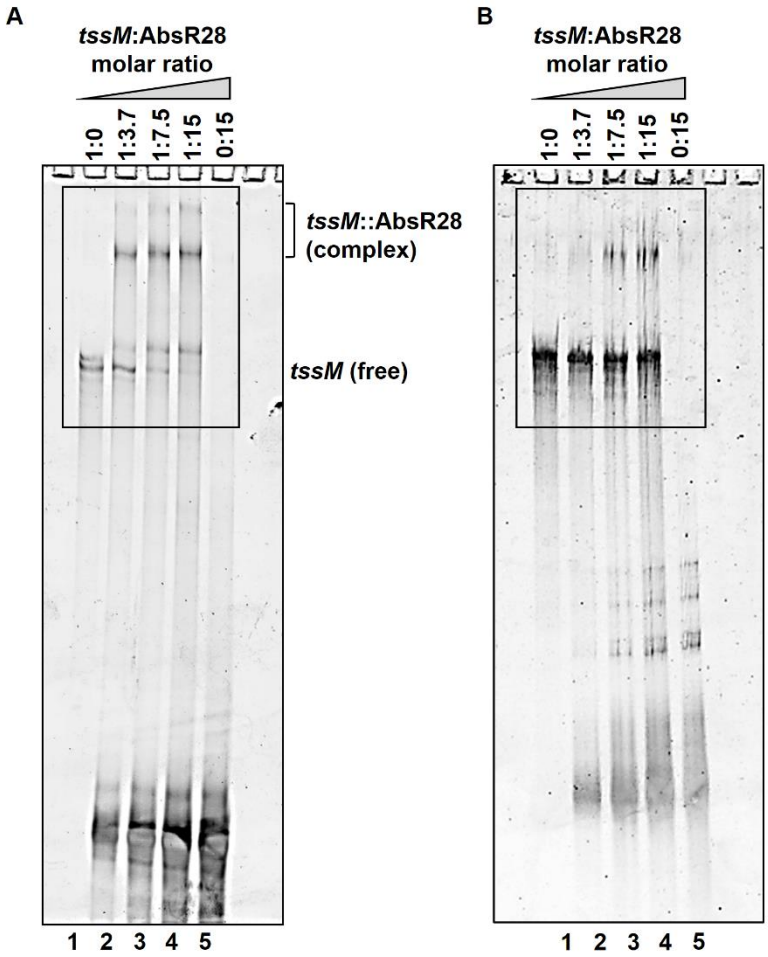

Figure S6

A

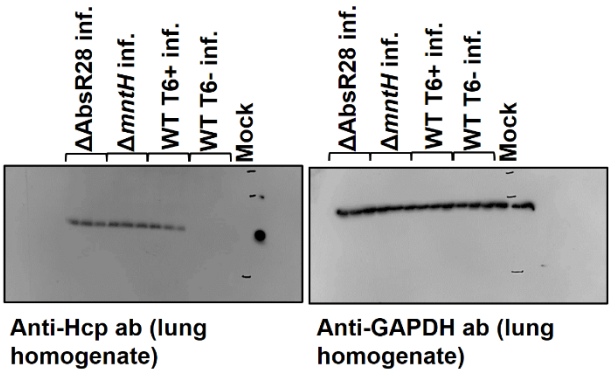

Figure S7

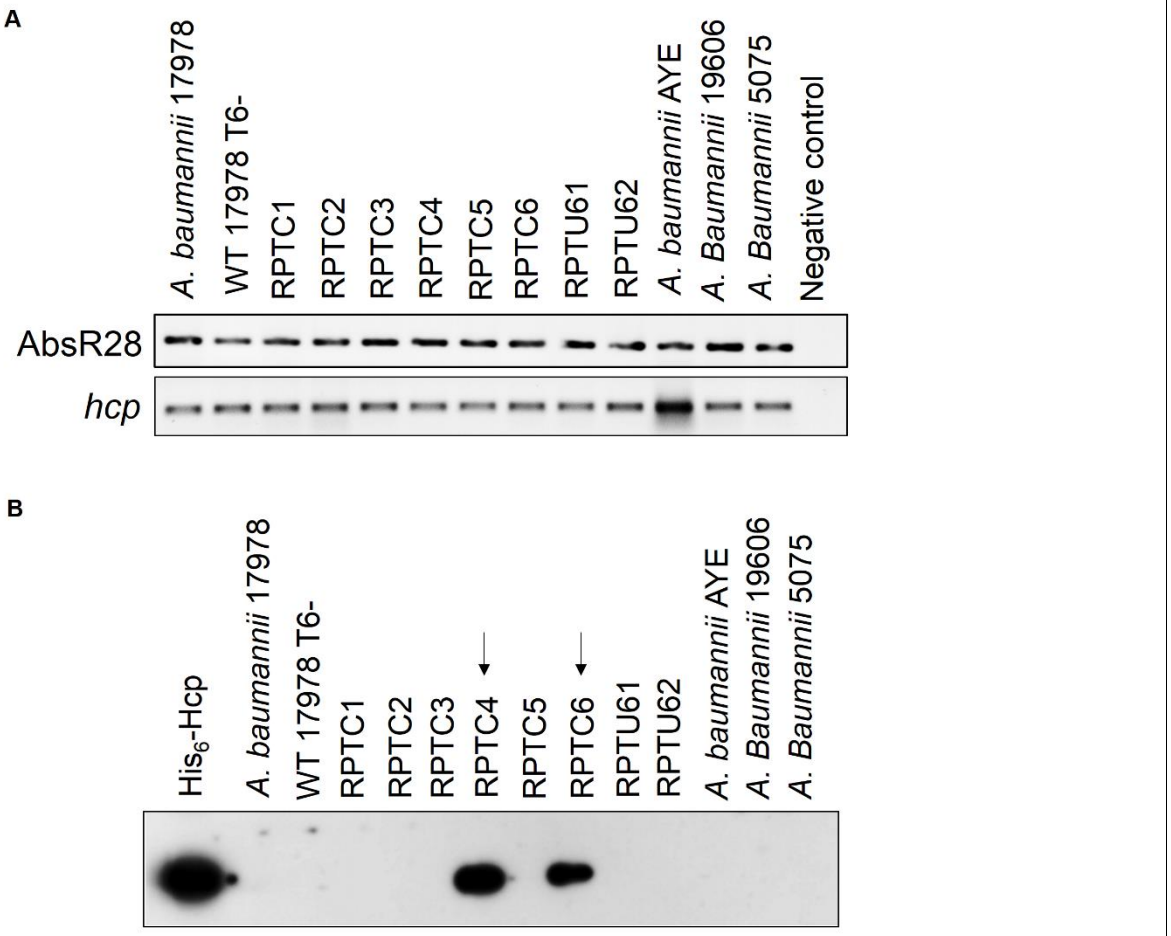

1264 **Figure S8**

Table 1. Oligonucleotides were used in this study. Related to Figures 1, 2, 3, 4, S2, S4, S5, S6, S7, and Methods.

Primer name	Sequence (5' - 3')	Description	Reference
UP437bpFPmntH	ATGCGTCGACAATTAACTGAAGTGGC	Forward primer for cloning *mntH* 437 bp upstream into pUC18	This study
UP437bpRPmntH	ACTCTAGATTAATGCGTTCCTCATCCATTTG	Reverse primer for cloning *mntH* 437 bp upstream into pUC18	This study
DN500bpFPmntH	ATGGTACCAGACGACATGAATTGATAAG	Forward primer for cloning *mntH* 500 bp downstream into pUC18	This study
DN500bpRPmntH	ATGGAATTCAACTCGTGCTTGCTCG	Reverse primer for cloning *mntH* 500 bp downstream into pUC18	This study
UP125bpFPmntH	ATGGGGAACAGGGAATCTTTGTCAT	Forward primer for the amplification of *mntH* 125 bp upstream	This study
DN125bpRPmntH	ACCAGCATGAAAACCACAAGCAAT	Reverse primer for the amplification of *mntH* 125 bp downstream	This study
UP498bpFPAbsR28	TAAGTCGACATATGCAACTACATTCATTGCTGC	Forward primer for cloning AbsR28 498 bp upstream into pUC18	This study
UP498bpRPAbsR28	TTATCTAGAGAACGGATTTTACCTGTTTT	Reverse primer for cloning AbsR28 498 bp upstream into pUC18	This study
DN501bpFPAbsR28	TATGGTACCAAATAAGAGAATAATTATGGGCAT	Forward primer for cloning AbsR28 501 bp downstream into pUC18	This study
DN501bpRPAbsR28	TATGAATTCCCTAAAGTGCCCAGCTGTTTT	Reverse primer for cloning AbsR28 501 bp downstream into pUC18	This study
UP126bpFPAbsR28	ATTAATTCCTTACGATCAAATGGATGTAAAACC	Forward primer for the amplification of AbsR28 126 bp upstream	This study
DN126bpRPAbsR28	TGTGCCATTTTCTTGAGTTGTTCAATACTT	Reverse primer for the amplification of AbsR28 126 bp downstream	This study
AprF-Bam	ATCAGGATCCGTCGACCTGCAGTTC	Forward primer for cloning Apr-FRT into pUC18	Lab stock
AprR-Kpn	ATGGTACCGTGTAGGCTGGAGCTGCTTC	Reverse primer for cloning Apr-FRT into pUC18	Lab stock
Kan FP pWBAD30	TTCGATCGGAACTTCAAGATCCCCTCAC	Forward primer for cloning Kanamycin resistance marker into pBAD30	Lab stock
Kan RP pWBAD30	TTCGATCGTTCTCGAGAAGTATAGGAACTTCAGAGC	Reverse primer for cloning Kanamycin resistance marker containing XhoI restriction site into pBAD30	Lab stock
pW FP	TGTCTCGAGGATCGTAGAAATATCTATGATTATC	Forward primer for cloning *A. baumannii* ori into pBAD30-kan^R	Lab stock
pW RP	TGTCTCGAGGGATTTTAACATTTTGCGTTGTTC	Reverse primer for cloning *A. baumannii* ori into pBAD30-kan^R	Lab stock
AbsR28 FP pWBAD30	AGGAATTCGTCAAAAACTTGATCTTTAG	Forward primer for cloning AbsR28 into pWBAD30-kan^R	This study

AbsR28 RP pWBAD30	CCCAAGCTTATTGTCCGAATAGGAATAAAAAAACCTAGCG	Reverse primer for cloning AbsR28 into pWBAD30-kan^R	This study
RT *mntH* FP	GCAGTTCGCGGTGGTATAGA	qRT-PCR forward primer for *mntH*	This study
RT *mntH* RP	TAGCTCAACGACTTCGCCAG	qRT-PCR reverse primer for *mntH*	This study
RT *znuB* FP	ATTTGAGGCTGCCAATAGCG	qRT-PCR forward primer for *znuB*	This study
RT *znuB* RP	AAACGATGCTTTGCTTGCCC	qRT-PCR reverse primer for *znuB*	This study
RT *tonB* FP	CCAGATCCATCGCCAAAACG	qRT-PCR forward primer for *tonB*	This study
RT *tonB* RP	GGGTTACGCGCACGTTAGTA	qRT-PCR reverse primer for *tonB*	This study
RT *tssB* FP	TCAGCGAATTCGACCTCCAC	qRT-PCR forward primer for *tssB*	Lab stock
RT *tssB* RP	GTACGCTCAAGCTCAGATGC	qRT-PCR reverse primer for *tssB*	Lab stock
RT *tssC* FP	GTTGGTGTGCTGCTATTCGC	qRT-PCR forward primer for *tssC*	This study
RT *tssC* RP	CTCTTTTTCACGGCGATCCG	qRT-PCR reverse primer for *tssC*	This study
RT *hcp* FP	CTTCAAGTAGTGTAGGCGGC	qRT-PCR forward primer for *hcp*	Lab stock
RT *hcp* RP	CCATTTGCACGATAGAAGTC	qRT-PCR reverse primer for *hcp*	Lab stock
RT *tssE* FP	GTGGGGCTTTCTACAGCCAA	qRT-PCR forward primer for *tssE*	This study
RT *tssE* RP	ACCCGTATTTGTCTTAGCCGAG	qRT-PCR reverse primer for *tssE*	This study
RT *tssF* FP	TAGTAGCTTGGCGAGACGTG	qRT-PCR forward primer for *tssF*	Lab stock
RT *tssF* RP	GATCACACGCCACTGTTCAC	qRT-PCR reverse primer for *tssF*	Lab stock
RT *tssG* FP	ACCTGGTGCAGTCCAACTTT	qRT-PCR forward primer for *tssG*	This study
RT *tssG* RP	AAAAAGCGCCTTGCCCTAAG	qRT-PCR reverse primer for *tssG*	This study
RT *tssM* FP	CTCCGGCAACCAATCAGTCT	qRT-PCR forward primer for *tssM*	This study
RT *tssM* RP	AGCTGTAATACGAGCACCCG	qRT-PCR reverse primer for *tssM*	This study
RT *paar* FP	TGGCTAGCCCTTACATTACG	qRT-PCR forward primer for *paar*	Lab stock
RT *paar* RP	CGTTTTATGCGCCGGACAAG	qRT-PCR reverse primer for *paar*	Lab stock
RT *tssH* FP	CTCGAGTGCAATTATGCAGGC	qRT-PCR forward primer for *tssH*	This study
RT *tssH* RP	CACAACTCTCATGCGCCCTA	qRT-PCR reverse primer for *tssH*	This study
RT *tssA* FP	CAATCGCGAGCAAGCAATGA	qRT-PCR forward primer for *tssA*	This study
RT *tssA* RP	GCTAACCATTCATGCAGCGG	qRT-PCR reverse primer for *tssA*	This study
RT *tssK* FP	GCAGACCCACGAGTTGATTC	qRT-PCR forward primer for *tssK*	Lab stock
RT *tssK* RP	CTCACACCCGAACGTACTGG	qRT-PCR reverse primer for *tssK*	Lab stock

RT *tssL* FP	TAACCCAGCAAGACCCAAGC	qRT-PCR forward primer for *tssL*	This study
RT *tssL* RP	TCGCTCTTTTCCACGACTACG	qRT-PCR reverse primer for *tssL*	This study
RT *vgrG* FP	TGACCGTCCGTTTGTAGTGG	qRT-PCR forward primer for *vgrG* (A1S_0550)	This study
RT *vgrG* RP	TGACCGCATGGCTACTTTGT	qRT-PCR reverse primer for *vgrG* (A1S_0550)	This study
RT *tetR1* FP	ATGCTGTACTGCCTTTGTCTCT	Forward primer to check for *tetR1* in pAB3	This study
RT *tetR1* RP	CCGTTTCGTGGTCCACACAT	Reverse primer to check for *tetR1* in pAB3	This study
RT *tetR2* FP	CAACCTCTTGGGCCAGTGTG	Forward primer to check for *tetR2* in pAB3	This study
RT *tetR2* RP	GGTCCACGTGCCACTGATAG	Reverse primer to check for *tetR2* in pAB3	Lab stock
RT AbsR1 FP	GGTTAAGTAAAGAATTTTAAAG	qRT-PCR forward primer for AbsR1	Lab stock
RT AbsR1 RP	CTCTACCGAAGCAAAAGC	qRT-PCR reverse primer for AbsR1	Lab stock
RT AbsR11 FP	AACGTAGCGGTGTCACATCA	qRT-PCR forward primer for AbsR11	Lab stock
RT AbsR11 RP	GGTGAAGAGTCCCATTCCCT	qRT-PCR reverse primer for AbsR11	Lab stock
RT AbsR25 FP	AAATCATGTGTAGGACCGAG	qRT-PCR forward primer for AbsR25	Lab stock
RT AbsR25 RP	AAAGCCTACTCAAGAAGCAG	qRT-PCR reverse primer for AbsR25	Lab stock
RT AbsR28 FP	AAGGAGGACATCATGCCAAC	qRT-PCR forward primer for AbsR28	Lab stock
RT AbsR28 RP	AATTCGAGCATTCGGACAAG	qRT-PCR reverse primer for AbsR28	Lab stock
RT AbsR29 FP	CGCAGTCAATCAATCAGTGCATTT	qRT-PCR forward primer for AbsR29	Lab stock
RT AbsR29 RP	GATGCAAAGAGCTTGCCAAT	qRT-PCR reverse primer for AbsR29	Lab stock
RT *hfq* FP	CCTTGACTACCACCCTGAGC	qRT-PCR forward primer for *hfq*	Lab stock
RT *hfq* RP	TCTACAGTTGTTCCAGCTCGT	qRT-PCR reverse primer for *hfq*	Lab stock
RT 16s FP	AGAGGGTGCGAGCGTTAATC	qRT-PCR housekeeping gene forward primer	Lab stock
RT 16s RP	GTTAAGCTCGGGGATTTCAC	qRT-PCR housekeeping gene reverse primer	Lab stock
RT A1S_2838 FP	GGCACCATTCGTAGGTGGTT	Forward primer to check the polar effect of ΔAbsR28 upstream	This study
RT A1S_2838 RP	AGCGGAATCGTCTTCTTCGG	Reverse primer to check the polar effect of ΔAbsR28 upstream	This study
RT A1S_2839 FP	ATCCGGGTCTTGTCCGAATG	Forward primer to check the polar effect of ΔAbsR28 downstream	This study
RT A1S_2839 RP	CCTGAATGGAGCATCACCCA	Reverse primer to check the polar effect of ΔAbsR28 downstream	This study
AbsR28 IVT FP	CCGGAATTCTAATACGACTCACTATAGGGAGATTTTCAACGGCAC	Forward primer for AbsR28 in vitro transcription	This study
AbsR28 IVT RP	CCCAAGCTTATTGTCCGAATAGGAATAAAAAAACCTAGCG	Reverse primer for AbsR28 in vitro transcription	This study

FP IVT *tssM*	TAATACGACTCACTATAGGGGTTTGCACAAACATCTGTTGAACCA	Forward primer for *tssM* in vitro transcription	This study
RP IVT *tssM*	CGTACTCTGCTTGGGTATCCTTTT	Reverse primer for *tssM* in vitro transcription	This study

Table 2. Bacterial strains were used in this study.

Bacterial strains	**Source**	**Identifier**
Acinetobacter baumannii ATCC 17978	ATCC	WT
Acinetobacter baumannii ATCC 17978 T6-	This study	WT T6-
Acinetobacter baumannii ATCC 17978 T6+	This study	WT T6+
Acinetobacter baumannii ATCC 17978 Δ*mntH*	This study	Δ*mntH*
Acinetobacter baumannii ATCC 17978 ΔAbsR28	This study	ΔAbsR28
Acinetobacter baumannii ATCC 17978 ΔAbsR28-pWBAD30	This study	ΔAbsR28-pWBAD30
Acinetobacter baumannii ATCC 17978 ΔAbsR28-pWBAD30AbsR28	This study	ΔAbsR28-pWBAD30AbsR28
Acinetobacter baumannii ATCC 17978 Δ*tssM*	R.P. lab	Δ*tssM*
Escherichia coli DH5α	Invitrogen, USA	*E. coli* DH5α
Escherichia coli DH5α-pNYL GFP	Prof. N.K. Navani, IIT Roorkee, India	*E. coli*-pNYL GFP
Escherichia coli J53	Dr. Sanath Kumar H, ICAR-CIFE, India	*E. coli* J53
Pseudomonas aeruginosa PAO1	Prof. N.K. Navani, IIT Roorkee, India	*P. aeruginosa*

Table 3. Plasmids were used in this study.

Plasmids	**Source**	**Identifier**
pUC18	Thermo Scientific, USA	N/A
pUC18-UP*mntH*-AprFRT-DN*mntH*	This study	N/A
pUC18-UPAbsR28-AprFRT-DNAbsR28	This study	N/A
pMDIAI	Addgene	N/A
pAT02	Prof. Bryan Davies, University of Texas, San Antonio, USA	N/A
pAT03	Prof. Bryan Davies, University of Texas, San Antonio, USA	N/A
pKD4	(Datsenko and Wanner, 2000)	N/A
pBAD30-amp^R	Prof. Eric D. Brown, McMaster University, Hamilton, ON	N/A
pBAD30-kan^R	This study	pBAD30
pWBAD30-kan^R	This study	pWBAD30
pWBAD30-kan^R-AbsR28	This study	pWBAD30-AbsR28